White Rose Research Online

eprints@whiterose.ac.uk
https://eprints.whiterose.ac.uk
Universities of Leeds, Sheffield and York

Deposited via The University of Leeds.

White Rose Research Online URL for this paper:
https://eprints.whiterose.ac.uk/id/eprint/171030/

Version: Accepted Version

**Article:**
McArthur, AD, Bailleul, J, Mahieux, G et al. (2021) Deformation–sedimentation feedback and the development of anomalously thick aggradational turbidite lobes: Outcrop and subsurface examples from the Hikurangi Margin, New Zealand. Journal of Sedimentary Research, 91 (4). pp. 362-389. ISSN: 1527-1404

https://doi.org/10.2110/jsr.2020.013

This item is protected by copyright. This is an author produced version of an article published in Journal of Sedimentary Research. Uploaded in accordance with the publisher's self-archiving policy.

**Reuse**
Items deposited in White Rose Research Online are protected by copyright, with all rights reserved unless indicated otherwise. They may be downloaded and/or printed for private study, or other acts as permitted by national copyright laws. The publisher or other rights holders may allow further reproduction and re-use of the full text version. This is indicated by the licence information on the White Rose Research Online record for the item.

**Takedown**
If you consider content in White Rose Research Online to be in breach of UK law, please notify us by emailing eprints@whiterose.ac.uk including the URL of the record and the reason for the withdrawal request.

UNIVERSITY OF LEEDS
University of Sheffield
UNIVERSITY of York

Accepted article in Journal of Sedimentary Research; DOI 10.2110/jsr.2020.013

# Deformation-sedimentation feedback and the development of anomalously thick aggradational turbidite lobes: outcrop and subsurface examples from the Hikurangi Margin, New Zealand

McArthur, A.D.[1*], Bailleul, J. [2], Mahieux, G.[3], Claussmann, B.[2,4], Wunderlich, A.[5], McCaffrey, W.D.[1]

1. School of Earth and Environment, University of Leeds, Leeds, LS2 9JT, United Kingdom

2. U2R 7511, Basins-Reservoirs-Resources (B2R), Geosciences department, UniLaSalle, 60026, Beauvais, France

3. U2R 7511, Basins-Reservoirs-Resources (B2R), Université de Picardie Jules Verne, 80039, Amiens, France

4. Schlumberger, Software Integrated Solutions, London, SW1E 6AJ, United Kingdom

5. OMV New Zealand Ltd, The Majestic Centre, 100 Willis Street, 6011 Wellington, New Zealand

* Email: a.mcarthur@leeds.ac.uk

## ABSTRACT

Concepts of the interaction between autogenic (e.g., flow process) and allogenic (e.g., tectonics) controls on sedimentation have advanced to a state that allows the controlling forces to be distinguished. Here we examine outcropping and subsurface Neogene deep-marine clastic systems that traversed the Hikurangi subduction margin via thrust-bounded trench-slope basins, providing an opportunity to examine the interplay of structural

deformation and deep-marine sedimentation. Sedimentary logging and mapping of Miocene outcrops from the exhumed portion of the subduction wedge record heavily amalgamated, sand-rich lobe complexes, up to 200 m thick, which accumulated behind NE-SW orientated growth structures. There was no significant deposition from low-density parts of the gravity-flows in the basin centre, although lateral fringes demonstrate fining and thinning indicative of low-density flow deposits. Seismic data from the offshore portion of the margin show analogous lobate reflector geometries. These deposits accumulate into complexes up to 5 km wide, 8 km long and 300 m thick, comparable in scale with the outcropping lobes on this margin. Mapping reveals lobe complexes that are vertically stacked behind thrusts. These results illustrate repeated trapping of the sandier parts of turbidity currents to form aggradational lobe complexes, with the finer-grained suspended load bypassing to areas downstream. However, the repeated development of lobes characterised by partial bypass implies that a feedback mechanism operates to perpetuate a partial confinement condition, via rejuvenation of accommodation. The mechanism proposed is a coupling of sediment loading and deformation rate, such that load-driven subsidence focuses stress on basin bounding faults and perpetuates generation of accommodation in the basin, hence modulating tectonic forcing. Recognition of such a mechanism has implications for understanding the tectono-stratigraphic evolution of deep-marine fold and thrust belts and the distribution of resources within them.

**Keywords:** lobe complexes; Neogene; deep-marine; trench-slope basin; tectono-stratigraphic; feedback mechanism

## INTRODUCTION

Understanding the interaction between autogenic and allogenic controls is a current research focus in sedimentology (Burgess et al., 2019). Autogenic or inherent controls are

those within the system, such as flow process or local structure development (e.g., Covault et al., 2007; Picot et al., 2016), whilst allogenic controls are external to the sedimentary system, such as sediment supply or regional tectonics (e.g., Prelat and Hodgson 2013; Soutter et al., 2019). The geomorphology resulting from structural deformation influences accommodation and whether a deep-marine sedimentary system is fully confined (e.g., Sinclair and Tomasso 2002; Marini et al, 2015, 2016a, b), partially confined, with potential for downstream bypass (e.g., Deptuck et al., 2008; Casciano et al., 2019; McArthur and McCaffrey 2019), or unconfined, with unrestricted run-out of flows (e.g., Normark, 1978; Normark et al., 1983; Clift et al., 2002; Jegou et al., 2008; Savoye et al., 2009). Submarine lobe deposits demonstrate a range of dimensions and stacking patterns depending on this confinement, with lateral offset stacking demonstrated in unconfined settings (e.g., Prelat et al., 2010; Brunt et al., 2013; Spychala et al., 2017; Maselli et al., 2019), or more complex stacking patterns in fully- to partially-confined settings (e.g., Haughton, 2000; Etienne et al., 2012; Spychala et al., 2015; Tinterri and Tagliaferri, 2015). Regardless of setting, lobe complexes typically do not grow beyond tens of metres in thickness before shutdown or lobe avulsion (Prelat et al., 2010; Macdonald et al., 2011; Straub and Pyles, 2012). In highly- to fully-confined settings, lateral migration may not be possible, leading to the formation of ponded, sheet-like turbidites (Sinclair and Tomasso 2002; Marini et al, 2015, 2016a, b). In such settings, the co-deposition of most or all of the finer grained suspended load in association with coarser sediment fractions commonly leads to the formation of muddy caps to successive sandy event beds (Patacci et al., 2015; Marini et al. 2016b; Dorrell et al., 2018).

When confinement is tectonically controlled, it is thought that interaction of successive turbidity currents with evolving seafloor structures may result in the development of more complex deposits in terms of thickness and co-deposition of different grain size classes (e.g., Sinclair and Tomasso, 2002; Brunt et al., 2004, Noda, 2018; Butler, 2019;

Soutter et al., 2019). However, the sparsity of both outcrop and subsurface studies of such confined systems limits our understanding of the interplay between sedimentary and tectonic processes and the effects upon the resulting stratigraphic architecture. Here, we address this knowledge gap by documenting both outcropping and subsurface systems from trench-slope basins of the Hikurangi subduction margin, on and offshore of the North Island of New Zealand (Fig. 1). Only by integrating high resolution, bed-scale sedimentological outcrop studies with large-scale 3D seismic analysis from the same area can we get a full understanding of the stratigraphic architecture, basin structure and system evolution. In this fold and thrust belt setting, Neogene lobe complexes adjacent to growth structures are anomalously thick (>200 m) and form highly amalgamated, sand-rich sequences within dominantly silt to mudstone prone basins. Specific objectives are to: 1) integrate studies of high-resolution outcrop and large-scale seismic architectures to interpret the geological processes (sedimentary and structural) and depositional setting capable of perpetuating bed amalgamation during the accumulation of thick, sand-rich lobe complexes deposited in tectonically active settings; 2) consider the variable influence of auto- and allogenic controls on the development of deep-marine lobe complexes in areas of active seafloor deformation; 3) develop a depositional model for the interaction of deep-marine sedimentation and active structure growth on submarine slopes; 4) assess the implications for the timing and distribution of syn-kinematic lobe complex development in deep-marine fold and thrust belts.

Development of such understanding is important as submarine lobes may act as carbon sinks (e.g., Rabouille et al., 2019), host hydrocarbon reservoirs (e.g., Prather, 2003; Saller et al., 2008), and reservoirs for low carbon initatives, such as carbon capture and storage.

## GEOLOGICAL SETTING

This work concerns the Miocene to Recent sequence of the Hikurangi subduction margin (Fig. 1). Prior to the onset of Cenozoic subduction, Zealandia was largely submerged (Reyners, 2013; Strogen et al., 2014), with widespread deposition of Paleogene deep-marine carbonates and marls (Fig. 2; Lillie, 1953; Chanier and Ferriere, 1991). Hikurangi subduction began ca. 25 Ma, associated with the convergence of the Pacific and Australian plates (Rait et al., 1991; Nicol et al., 2007; Reyners, 2013). The overriding Australian Plate has undergone significant internal deformation throughout the Neogene, resulting in the development of dominantly ENE-WSW-trending reverse faults with subsidiary normal and strike-slip faulting (Fig. 1; Chanier and Ferriere, 1991; Beanland et al., 1998; Nicol et al., 2007; Barnes et al., 2010), and of NE-SW elongated fold and thrust-bounded trench-slope basins (Bailleul et al., 2013; McArthur et al., 2019). Although a general migration of deformation towards the trench is seen, emplacement of thrusts and folds was out of sequence (Chanier & Ferriere 1991; Bailleul et al. 2013).

Three phases of deformation have been documented during the Neogene, which can be associated with the response of the overriding plate to changes in the style of subduction (Fig. 2; Wells, 1989; Chanier and Ferriere, 1991; Nicol et al., 2007). These phases correspond to: 1) compression, uplift and associated emplacement of thrust nappes in the latest Oligocene to Early Miocene related to the onset of subduction (Chanier and Ferriere, 1991; Rait et al., 1991); 2) a mixed phase of tectonic collapse-related extension and continued convergence during the Middle to Late Miocene, resulting in normal faulting on the margin (Chanier et al., 1999; Barnes et al., 2002; Bailleul et al., 2013); 3) resumption of margin-wide compression from the latest Miocene to present. The last phase is responsible for the development of the modern margin, with uplift and exhumation of the North Island Axial and Coastal Ranges, the latter corresponding to the western, exhumed, inner portion of the subduction wedge (Fig. 3; Nicol and Beavan, 2003; Litchfield et al., 2007; Nicol et al., 2007; Bailleul et al., 2013;

Jiao et al., 2015). The evolution of the subduction wedge can be traced by the infill of the trench-slope basins, the innermost of which have a Miocene aged fill, with progressively younger sediments towards the Hikurangi Trench (Fig. 2; Lewis and Pettinga, 1993).

The Plio-Pleistocene history of the margin not only records significant uplift, due to acceleration of subduction, but also shortening within the fold and thrust belt, as well as frontal accretion at the trench (Barnes and de Lepinay, 1997; Beanland et al., 1998; Nicol et al., 2002; Litchfield et al., 2007; Reyners et al., 2011; Barnes et al., 2018). Offshore, the subduction wedge displays a stepped profile, with trench-slope basins evolving on the back limbs of thrust-cored structural highs (Lewis and Pettinga, 1993; Barnes et al., 2010).

Thin-skinned deformation on the trench-facing side of the upper plate resulted in dominantly deep-marine sedimentation in the trench-slope basins (Nicol et al., 2007; Burgreen and Graham, 2014). The stratigraphic record is punctuated by a series of unconformities and episodes of syn-sedimentary deformation, indicative of a strong tectonic influence on the sedimentation (Neef, 1992; Bailleul et al., 2007, 2013; Burgreen-Chan et al., 2016). The fill of the trench-slope basins includes deep-marine mudstones, siltstones, turbidites, mass-transport deposits and carbonates (Fig. 2; Lee and Begg, 2002). Typically, the fill of the outcropping basins consists of regularly bedded, mud-rich turbidites, as well as shallow-marine fringes (Bailleul et al., 2007). Although tortuous paths of sediment transport may be expected on such margins, this is not always the case, as observed here (McArthur and McCaffrey, 2019; Crisostomo Figueroa et al., 2020) and other subduction margins (e.g., Cascadia [Nelson et al., 2000] or the Makran [Bourget et al., 2011]), where transverse channels may bypass significant portions of the slope.

Specifically, we examine outcropping Lower Miocene strata of the Greenhollows Formation (Fig. 2), which was estimated at 370 m thick by Neef (1992) or 600 m by Francis

and Johansen (2011), implying a large degree of thickness variation across the basin (Fig. 3; Bailleul et al., 2007). In the study area, these syn-subduction strata outcrop within the Akitio Syncline (Neef, 1992), which is bounded to the southeast by the Coastal Block and to the northwest by the Pongaroa Block (Fig. 3). The western limb of this syncline is transected by the N-S trending Breakdown Fault Zone (Fig. 3; Neef, 1992, Malié et al., 2017), whereas further north, second order folding is expressed by the Auster and the Paripapa synclines, separated by the Kawakawa Anticline (Fig. 3; Lee and Begg, 2002). The outcrops correspond to the preserved portion of the Miocene Akitio trench-slope basin (Bailleul et al., 2007). The multi-phase tectonic history not only controlled the sediment distribution within that area, but also the successive migration and deformation of the basin edges, as well as subsequent erosion (Bailleul et al., 2013). To the southeast of Pongaroa, the Greenhollows Formation shows extensional structures associated with the Middle to Late Miocene episode of deformation (Malié et al., 2017). These normal faults and small-scale grabens are overprinted by thrusts and reverse faults resulting from the third phase of deformation, with a shortening also responsible for the larger scale folding and uplift of the entire area (Bailleul et al., 2013).

In the subsurface, we examine the structure and fill of the Porangahau Trough and adjacent structural ridges (Fig. 1). Based upon regional seismic mapping and ties to nearby wells this basin fill is interpreted as Late Miocene to Recent in age (McArthur and McCaffrey, 2019). The trough is aligned NE-SW, bounded to the NW by the Madden Fault and to the SE by the Porangahau Fault (Fig. 2). The structure appears simpler than the more mature onshore basin, with purely convergent structures reported in this basin (Barnes et al., 2010; McArthur et al., 2019), which is younger than the phase of extension reported in the interior of the margin. The basin fill was dominantly sourced from the palaeo-Madden Canyon (McArthur and McCaffrey, 2019) and preserves up to 2 km of sediments, with the focus here on ca. 300 m of reflectors in the middle of the basin fill.

168 # METHODS

169 ## *Outcrop sedimentology*

170 We examine the Lower Miocene (Burdigalian) succession of the Akitio Basin (Fig. 3),
171 with fieldwork conducted to characterise the lithofacies, stratigraphic architecture and
172 depositional environments. Field mapping data were recorded with a Trimble® TDC100
173 (Fig. 3). Sedimentary logging was conducted at bed scale (1:50), across seven sections,
174 totalling 542 m (Fig. 3). Three hundred and fifty-five palaeocurrent indicators were measured
175 from three-dimensional ripples, flute casts, tool marks and primary current lineations. A
176 lithofacies scheme was developed and lithofacies associations were used to group similar
177 packages of sediments, metres to hundreds of metres thick. These data were supplemented by
178 information from micropalaeoentological analysis conducted by GNS Science New Zealand
179 to define the age of deposition and depositional environment. Samples were taken from
180 hemipelagic mudstone to avoid dating potentially reworked microfossils. Photographs of key
181 outcrops were taken to document the stratigraphic architecture, assisted by drone
182 reconnaissance using a DJI™ Mavic Pro. Digitally mapped lithofacies associations were
183 integrated with aerial photographs (courtesy of Land Information New Zealand – LINZ),
184 existing biostratigraphic information (The Fossil Record Electronic Database
185 [https://fred.org.nz/]) and petrophysical data (see below) in order to correlate and determine
186 the stratigraphic distribution of the depositional elements.

187 ## *Outcrop gamma-ray spectrometry*

188 Rock surfaces were cleaned with a rock pick, pry-bar, drilling hammer and brush to
189 remove the first 5 cm of the weathering surface. Natural gamma radiation was measured
190 using a Gr320 enviSPEC Portable Gamma-ray Spectrometer. The Gr320 records total counts
191 and ppm of 40K, 238U and 232TH during a pre-selected counting period of 120 seconds. The

same machine and technique as described by Braaksma et al. (2003) was used. During measurement the detector was placed perpendicular to the bedding. Measurements were made every 50 cm where possible to relate the petrophysical properties to geological parameters. Due to the edge effect and the 84 cm sampling radius of the sensor, efforts were made to measure within beds >84 cm thick. However, where not possible, beds <84 cm thick were measured; these data may have interference from adjacent beds. In combination with the sedimentology and palaeoentology, the data can help to refine interpretations of the depositional system (Slatt et al., 1992).

### *Seismic data*

Depth-converted 3D seismic data acquired at broadband frequency in 2017 by WesternGeco was used to assess the structure and stratigraphic architecture of offshore trench-slope basins. Data were interpreted using Schlumberger's Petrel© E&P and Eliis' Paleoscan™ software platforms; full stack data are displayed in SEG positive, such that a downward decrease in acoustic impedance is represented by a trough and a downward increase is represented by a peak. This study focuses on the Madden Channel area, located in the western part of the 3D seismic survey (Fig. 1). Major faults and structures were interpreted and regional surfaces were extrapolated from the 3D survey; two well ties enabled the base Pliocene reflector to be picked by correlation through 2D surveys (Fig. 1 and 2). Attribute mapping was used to create root-mean-square (RMS) of amplitude horizon maps through the interval of interest.

## FACIES AND ASSOCIATIONS

### *Lithofacies*

Detailed sedimentary logging permitted seven lithofacies to be identified based upon their composition, primary grain size, bed thickness and lateral continuity (Table 1). These comprise tabular, medium to thick-bedded, fine-grained sandstones (LF1); lenticular, thick-bedded, fine-grained sandstones (LF2); discontinuous thin- to medium-bedded sandstones and siltstones (LF3); tabular thin- to medium-bedded, fine-grained sandstones, siltstones and mudstones (LF4); alternations of fine-grained argillaceous sandstones and mud-clast conglomerates (LF5); beds of coarse bioclastic material (LF6); and massive marine mudstones (LF7).

*Lithofacies associations*

Associations of the lithofacies are grouped into packages of related strata, to identify stratigraphic architecture and associated depositional environments. Below, the three principal lithofacies associations (lobe axis, lobe fringe and mass-transport deposits) are described, then interpreted in sequence.

**Lithofacies Association 1 (LA1) – Lobe axis. ---**

Observations: Lithofacies Association 1 (LA1; Fig. 4) is characterised by tabular, thick-bedded, typically amalgamated and often-dewatered sandstones (LF1), with rare turbidite fines (LF4), often interbedded with discontinuous thin-beds (LF3), lenticular, thick-bedded sandstones (LF2) and very rarely argillaceous sandstones and genetically-related conglomerates (LF5). Occasionally beds of coarse bioclastic material (LF6) are also seen, typically underlying thicker sandstones (LF1); most beds show disseminated plant debris. This association is often amalgamated into packages tens to hundreds of metres thick (Fig. 5), of vertically stacked, high net to gross (N:G) deposits. Sandstones often show internal scours, grain-size breaks and mud-clasts aligned along horizons, indicating amalgamation of beds (Fig. 4C). Bioturbation is typically restricted to the rare mud-caps and includes large burrows

238 such as *Ophiomorpha* sp. and *Thalassinoides* sp. Sole marks and other traction structures are
239 rare but generally show a south-easterly palaeocurrent direction, with a mean of 135°. In the
240 Akitio Basin this association is seen on the preserved SE edge of the basin, where this
241 association can be mapped over 12 km$^2$ (Fig. 3). Logged sections L1 and L2 provide two
242 transects through this association, converging towards the top of these logs in the Owahanga
243 Gorge area (Figs. 3 and 5). The lower logged sections total to 98 m thickness (Logs 1-2 in
244 Fig. 5), but only cover the well-exposed interval. The overlying section is poorly-exposed and
245 occurs along a the Owahanga River, with sporadically outcropping sandstones totalling a
246 further 75 m of strata. A final well-exposed section covers 22 m of strata (Log 3 in Fig. 5),
247 such that LA1 is 195 m in thickness in this locality. Although LA1 appears as a relatively
248 homogenous, sand-rich association, the gamma ray response demonstrates some distinct
249 trends, with peaks and troughs that may be used to aid lateral correlations with the coeval
250 LA2 (Fig. 5).

251 Interpretations: Supported by the observations and interpretation of the laterally
252 adjacent LA2 (see below), these laterally extensive, tabular, often amalgamated sandstone
253 dominated deposits are interpreted as a ca. 200 m thick, vertically superimposed stack of
254 submarine lobe complex axes (*sensu* Prelat et al., 2009). The apparent absence of lateral
255 offset stacking indicates that successive lobe depocentres were fixed in the same locality.
256 Although aggradational lobe complexes have been recognised elsewhere (e.g., Prather et al.,
257 1998; Spychala et al., 2017), they develop thicknesses that are substantially less than those
258 demonstrated here, before avulsion or abandonment of the system terminates turbidite
259 deposition (der Merwe et al., 2014). Palaeocurrent directions to the SE indicate that the flow
260 was perpendicular to the NE-SW trending basin edge (Fig. 3), which was likely less than 2
261 km away during deposition (Bailleul et al. 2013). Very thin or absent mud-caps imply
262 downstream bypass of suspended fines; rare thin-bedded turbidite intervals exhibit signs of

sustained, rather than waning flow. More commonly, repeated erosion of the upper surfaces of turbidites resulted in the development of an amalgamated series of sandstones (Stow and Johansson, 2000). However, no significant scour surfaces were seen here, nor partially preserved thicker mud-caps.

Micropalaeontology samples from this association indicates a late Burdigalian age and deposition in mid-bathyal depths (>700 m). Without sedimentological evidence of shut down of the lobe system, individual lobe complexes are not immediately evident in outcrop. However, in the spectral gamma ray log a series of sharp based units with repeated decreasing log response permit the definition of multiple lobe complexes (Fig. 5), with the maximum thickness of any individual lobe complex being 80 m (Fig. 5). Mechanisms to control this anomalously thick accumulation of lobe sediments in this confined, tectonically active setting are discussed below.

**Lithofacies Association 2 (LA2) – Lobe fringes. ---**

Observations: This association comprises tabular thin-bedded turbidites (LF4), with sporadic thicker beds (LF1) separated by mudstones (LF7), hybrid beds (LF5) and rare lenticular sandstones (LF2) (Fig. 6). As with LA1, some beds may be associated with bioclastic grits (LF6) and most beds show disseminated plant debris. LA2 deposits are seen to grade up from LA1 (Fig. 5) or simply from thick intervals of LF7 (Fig. 7), occurring across the mapped Upper Burdigalian extent of the Akitio Basin (Fig. 3); i.e. this association is seen across the remainder of the contemporary basin fill where LA1 is not present. The thickness of this association is highly variable across the basin, with exposures ranging from tens to hundreds of metres in thickness (Fig. 7). Overall this association is more heterolithic, includes more hybrid event beds (LF5) and has a lower N:G, but exhibits less structures than LA1 (Fig. 8). Unlike LA1, some intervals of hemipelagic mudstone (LF7) up to 250 cm thick

287 are present (Fig. 7). Bioturbation is common to intense across all lithofacies and as with LA1
288 includes *Ophiomorpha* sp. and *Thalassinoides* sp, but rare to abundant *Chondrites* sp.,
289 *Nerites* sp. and *Phycosiphon* sp. are also identified. Sole marks and other structures exhibit
290 mean palaeocurrent directions similar to LA1 (142$^{o}$), but with a slightly wider spread (Fig. 8).
291 Where preserved, the top of this association is typically truncated by a basin-wide MTD (Fig.
292 3) (see LA3 below). Although showing a similar range of gamma ray responses to LA1
293 (typically around 20-30 counts per 120 seconds), the gamma ray character of this association
294 shows higher frequency changes in vertical log response than LA1 and distinct breaks in the
295 trend (Fig. 9).

296 Interpretations: These laterally extensive, sandstone-rich deposits are interpreted as
297 lateral lobe fringes (*sensu* Spychala et al., 2017). The decreased N:G, increased presence of
298 hybrid beds and lateral association with LA1 imply these sediments are not laterally
299 continuous, sheet-like deposits across the basin (e.g., Prather et al., 2012; Patacci et al.,
300 2015), but form the fringes to a lobe system (Prelat et al., 2009; Kane et al., 2017). Despite
301 showing mud-caps, these differ from the ponded turbidites of the underlying system in that
302 beds show slightly fewer traction structures, more variable palaeocurrent orientations,
303 interpreted to represent flow deflections and have a wider variety of bed thicknesses (Fig. 7
304 and 8; Bailleul et al., 2007). With run-out of flows towards the lobe fringes greater mudstone
305 deposition is inferred, as opposed to the bypass and potential erosion of bed tops in the axial
306 portion. The hemipelagic mudstone dominated intervals may represent periods of shutdown
307 (Fig. 7), i.e. they may separate seven different lobe complexes, which are harder to recognise
308 in the amalgamated axis (LA1), but discernible in the lobe fringe (LA2).

309 As with LA1, micropalaeontology samples from this association indicate a late
310 Burdigalian age and deposition in mid-bathyal depths (>700 m). It is clearer to divide the
311 deposits of LA2 than those of LA1 into lobe complexes. This can be done based upon their

sedimentology, with mudstone-dominated intervals between complexes (Fig. 7). The petrophysical measurements agree with the sedimentological division into seven lobe complexes, with each complex defined by peaks in the gamma ray total followed by gradual reduction, allowing correlations with LA1 (Fig. 9).

**Lithofacies Association 3 (LA3) – Mass-transport deposits. ---**

Observations: This association comprises clasts of all lithofacies, ranging from pebble size to tens of metres thick and tens to hundreds of metres long, forming jumbled packages, metres up to ca. 100 m thick (Fig. 6C). Commonly clasts are composed of LF3-4, or blocks of carbonate rocks, bioclastic sandstone (LF6) or mudstone (LF7). Rafts are generally internally coherent and good quality outcrops are required to identify the often-subtle juxtaposition of rafts and to observe basal shear zones or large-scale folding of rafts. The matrix is composed of silty mudstone and may contain floating bioclastic debris. The matrix may form from <20% to >80%, of the deposit, often grading within it. Where an obvious erosion surface and truncation of underlying strata is not present, careful measurement of bedding orientations between sheared zones may also help to distinguish this association from in-situ deposits. A relatively thin (<5 m thick) example of this facies association is seen to underlie LA1 at the base of log 1 (Fig. 5), whilst several thinner examples underlie the LA2 (Fig. 7). Both LA1 and LA2 are overlain by a single event (L3 shown in Fig. 5), which has a variable thickness across the basin of up to 100 m and shows an erosive base (Fig. 6).

Interpretations: These often seismic-scale intervals are interpreted as mass-transport deposits (MTDs), remobilising sediments deposited within the basins and on their edges. Bioclastic debris may have been derived from shallow-marine facies that periodically developed on the basin edges (Bailleul et al., 2007). The widespread occurrence of these deposits indicates that they filled or partially filled basins, as can be observed in modern

basins offshore New Zealand, such as the Paritu Basin (Mountjoy and Micallef, 2012). The largest MTDs appear to be associated with significant changes in both accommodation and subsequent basin evolution, with different facies associations seen above the major MTDs compared with those beneath them (see description of Middle Miocene strata in McArthur and McCaffrey, 2019), implying either the MTDs or events that triggered them were responsible for such changes. The large MTD overlying the sequence shows significant erosion into both LA1 and LA2 (Fig. 6). Although it is difficult to determine the amount of erosion, this may be greater in the axial portion, as described in the subsurface example below. Although MTDs are pervasive in New Zealand stratigraphy, we have confidence that the studied interval between the documented MTDs (i.e., LA1-2) is in-situ, demonstrating dip and strike consistent with the regional strata (unlike the MTDs), no signs of internal slide or scour surfaces and presenting coherent stratigraphy correlatable over distances, which is not possible in MTDs.

### *Seismic facies*

Although detail on the sedimentary systems is gained from outcrop studies, the large-scale nature of the stratal architecture is difficult to resolve. Therefore, a comparison with similar systems imaged in the subsurface is appropriate to observe the preserved extent of the deposits (Fig. 10) and help understand the tectono-stratigraphic evolution. Analysis of seismic reflection data from the same margin allows us to examine the fill of offshore trench-slope basins, in the actively developing portion of the subduction wedge (McArthur et al., 2019), specifically the Porangahau Trough (Fig. 1). To aid this workflow, packages of reflectors with similar characteristics are defined. Five seismofacies are interpreted based upon their seismic amplitude, frequency, termination style and internal character to represent background hemipelagic sedimentation (SF1); sheet-like sediments with alternating character

(SF2); submarine channel fills (SF3); lobe complexes (SF4); and mass-transport deposits (SF5) (see Table 2 and the following text for description and interpretation).

*Seismic facies associations*

Associations of the seismofacies can be grouped into packages of related reflectors, to identify stratigraphic architecture and basin setting. Below, the three principal seismofacies associations (SA) are described then interpreted, being pre-lobe strata (SA1), aggradational lobe complexes (SA2) and post-lobe strata (SA3). Attribute analysis was conducted to aid interpretation in the interval of interest (Fig. 12; supplementary video).

**Seismofacies Association 1 (SA1) – Pre-lobe strata. ---**

Observations: Seismofacies Association 1 (SA1) is characterised by low amplitude, low frequency, laterally continuous reflectors (SF1) and alternating high and low amplitude, low frequency reflectors (SF2) (Fig. 10). The faulted and folded reflectors that form the substrate to the trench-slope basins mostly comprise low amplitude, chaotic reflectors (deformed SF1; Fig. 10). Within these reflectors, several faults and folds are imaged, with the principal structures defining the edges or sills of the basins (Fig. 11). The sills are thus underpinned by thrust-cored detachment folds, which at present extends NNE-SSW some ca. 75 km laterally along the margin. The western structure has a vertical throw of 2.5 km but is complicated by several detachment horizons (Fig. 10); the eastern structure has a minimum vertical throw of 3 km, however erosion of the crest of the sill is apparent (Fig. 12). A sharp surface overlies and truncates these lower reflectors, above which are alternating mostly low amplitude reflectors of SF2 and subordinate SF1, which are laterally continuous across individual basins but onlap against the basin edges (Fig. 11A and B). No distinctive geomorphological features are seen in mapped 3D surfaces within these reflectors.

Interpretations: A series of thrust faults and associated folds can be seen in the highly deformed reflectors at depth (SF1), here interpreted to represent pre-subduction strata *sensu* McArthur et al. (2019). The sharp surface overlying these reflectors is interpreted as a regional unconformity, marking the onset of the effects of subduction in this area, creation of individual trench-slope basins and initiation of their infill (Fig. 10). Above this surface, reflectors of SF1 and SF2 are seen to pond within the basin centre and onlap the edges (e.g., Prather et al., 1998). That no sedimentary features are imaged within SA1 (i.e., channels, lobes etc.) implies these represent a low energy infill. Note that the structures within the pre-subduction interval penetrate and influence the geometry of this package, but not the overlying reflectors, implying that deformation became focused on the basin bounding structures during deposition of SA2 and stopped thereafter. The basin bounding sill is formed by a thrust-cored detachment fold. Given that it affects the seafloor today, the expression of the sill during deposition cannot be precisely constrained, although it is clear that it was forming a topographic barrier on the seafloor at the time of deposition and causing growth strata in the adjacent basin.

**Seismofacies Association 2 (SA2) – Aggradational lobe complexes. ---**

Observations: Overlying the laterally continuous reflectors are a series of reflectors that are discontinuous at basin scale, mostly represented by SF4 within the core of the basin, fringed by SF1, whilst SF3 and SF5 are present in the up-dip portion (Fig. 11). SF3 is represented by lenticular, concave-up units that are kilometres wide and hundreds of metres thick, seen to truncate underlying reflectors and that are filled with relatively heterogeneous reflectors (Fig. 11). A prominent expression of SF3 is seen to cut the up-dip structure (Fig. 11G and H). SF4 is represented by semi-continuous, mounded, convex-up, mostly high amplitude reflectors, which are seen to downlap at their fringes, forming a radial pattern approximately 8 km in diameter in front of the downstream sill as illustrated in Figure 11H.

Mapping of horizons and RMS amplitude extractions of horizons through the interval dominated by SF4 demonstrate a complex array of high amplitude reflectors immediately down-dip of the structure separating the Porangahau Trough from the basin immediately upslope (Fig. 12A). These reflectors can be separated into at least five separate packages, each tens of metres thick (varying laterally from ca. 20 to 70 m thick) and generally stacking vertically to over 300 m thick (Fig. 11). Within the high amplitude reflectors, isolated lenses, tens of metres wide and up to kilometres in length, extend out from the upstream (i.e., NW) structure across the high amplitude area (Fig. 12). Subsequent downstream basins only show low amplitude reflectors over this interval (Fig. 12). However, at least three such occurrences of similar successions of reflector packages are seen in other basins of the subduction wedge (Fig. 12A).

Interpretations: The discontinuous reflector packages above SA1 characterise a variety of depositional styles. The lenticular and erosional SF3 is interpreted to represent the fill of submarine channels (e.g., Mayall and Stewart, 2000). For example, a major channel complex is interpreted to cross-cut the up-dip structure and acted as the primary sediment conduit feeding the basin (Fig. 11; 12A); this being the ancient expression of the Madden Channel (Fig. 1). The first discontinuous deposits in the basin are clearly an MTD (Fig. 12B), however no significant megaclasts are resolved, thereby suggesting this MTD didn't form any significant seafloor topography.

The discontinuous, radial, downlapping reflectors of SF4 are interpreted as submarine lobe complexes (*sensu* Booth et al., 2003). At least four lobe complexes can be defined at the base of the intra-basinal palaeo-slope (Fig. 11, 12). These sediments were fed through the up-dip channel and stack vertically behind the downstream sill (Fig. 11; Fig. 12C), giving a sustained, aggradational stacking pattern, as the confinement did not allow for significant lateral offset stacking (*sensu* Prelat et al., 2009). This confinement and lack of lateral

433 migration may explain why the feeder channel fill is approximately the same width as the
434 lobe complexes. The radial pattern implies that along slope currents were not influential in
435 the basin at this time, as they later became (Bailey et al., 2020). The finger-like features seen
436 on RMS extractions of the lobes are interpreted as distributary channels (e.g., Fig. 11G; 12D;
437 Maier et al., 2020), which can be seen approaching the sill. Restriction of the high amplitude
438 responses to areas behind the sill implies that coarse-grained sediments were trapped behind
439 this growth structure (Fig. 12E). However, attribute extractions show an evolution of the
440 interaction with the sill during deposition of the lobes, with the first three complexes being
441 entirely trapped behind the sill (Fig. 12C, D and E), but eventually displaying a low
442 amplitude shadow across the sill and into the downstream accommodation, which could
443 imply bypass of fines (Fig. 12F). Ultimately, erosion of the sill's crest is seen (Fig. 12F) and
444 higher amplitudes begin to develop in the basin downstream, which may have occurred due
445 to overspill and bypass of coarser material.

446 **Seismofacies Association 3 (SA3) – Post-lobe strata. ---**

447 Observations: The radial reflectors of SA2 are terminated by a chaotic interval of SF5
448 tens of metres thick (Fig. 11). The deposits of SF5 are seen to have both been sourced
449 through the feeder conduit and also to have been shed from the flanks of the basin bounding
450 structures (Fig. 12G). Those fed through the up-dip conduit appear to truncate the proximal
451 deposits of SF4, whilst those from the local structures simply overly SF4. Above this,
452 alternating reflectors of SF1, 3 and 5 combine to fill the basin to the seafloor.

453 Interpretations: Ultimately the whole system was significantly modified after the
454 emplacement of a major MTD over the lobe complexes, which shows great erosion into the
455 axial portion of the lobes, either directly preceding or contemporaneous to the MTD
456 emplacement (Fig. 12G). This MTD was sourced remotely and fed through the same channel

system that supplied the lobe complexes. Emplacement of additional smaller, lateral MTDs is thought to relate to local collapse of the up-dip structure and may indicate a renewed phase of deformation.

Lobe deposition is inferred to have been terminated either as a result of MTD emplacement, which potentially damned the upstream channel (c.f., McArthur and McCaffrey, 2019), or by a change in the deformation style, due to the associated diversion of the sediment dispersal pathway elsewhere (c.f., McArthur et al., 2019). Alternatively, the sediment supply could simply have been switched off. Recurrences of channel complexes (SF3) above lobe systems implies that basin filling and development of bypass conduits connecting to downstream basins is a common phenomenon (Fig. 11), as is seen in the outcropping succession (McArthur and McCaffrey, 2019), with relatively unconfined MTDs, hemipelagites and contourites providing the overburden (Bailey et al., 2020).

## INTEGRATION AND INTERPRETATION OF TECTONO-STRATIGRAPHIC ARCHITECTURE

Distinctive patterns of sedimentation can be observed in detail at outcrop, at larger scale in seismic data and integrated to leverage a clearer understanding of the tectono-stratigraphic evolution of confined intra-slope basins. At outcrop scale, the petrophysical data enable a correlation of the lobe axis and fringe deposits to be made (Fig. 9), which implies that a greater thickness of fringe deposits is preserved within the outcropping basin than at the axis. A similar thickness discrepancy is seen from axis to fringe deposits in the subsurface example, with the lobe axis being incised and eroded (Fig. 11 and 12). This may be a result of erosion over the position of the lobe axis by the overlying MTD or due to periods of sustained bypass of fines during deposition of coarser-grained axial deposits. A combination

480 is likely, with lateral correlation of the more bypass prone axial complexes to thicker
481 intervals of fringe deposits (Fig. 9).

482 In both outcrop and subsurface examples, lobe complexes of similar dimensions
483 (hundreds of metres thick [minimum 10 m, maximum 70 m] by approximately 15 $km^2$; Figs.
484 3 and 12), overlie older, ponded sediments, indicating that the basins had formed and seafloor
485 relief had been generated by structural activity, both within the basins and on their edges
486 (Fig. 3; 11). The deposition of the lobes suggests that the deformation became focused on the
487 basin bounding structures, with intra-basinal structures no longer exerting an influence on the
488 seafloor. Even if it is difficult to establish at outcrop, this is clearly seen in the subsurface,
489 where reflectors of SA1 were deformed and vary in thickness adjacent to structures, whilst
490 those of SA2 are not deformed (Fig. 10). Although both outcrop and subsurface examples
491 shown in this study overlie muddy MTDs they are not significantly thick, being <5 m at
492 outcrop and ca. 20 m thick in the subsurface, nor do they include megaclasts; therefore, large-
493 scale ponding on top of these MTDs is not envisaged.

494 At the time of lobe inception, the basin-bounding structures were still exerting an
495 influence on the seafloor, as illustrated by the trapping of the coarse sediment within these
496 depocentres (Fig. 3; 12). However, both at outcrop and in the subsurface, the clastic sediment
497 dispersal system did not terminate with the sandstone component of the lobes (e.g.,
498 Boulesteix et al., 2019), and not even within the same basin as where the lobes were
499 deposited (Fig. 12). The lobes in outcrop do not show a frontal fringe, but show palaeoflow
500 towards the basin sill (Fig. 8). In the subsurface a continuation of lower amplitude reflectors
501 across and over the downstream sill is seen in amplitude mapping, implying the bypass of
502 fines beyond the high amplitude lobe axis (Fig. 12A and F). Therefore, although the coarse-
503 grained component was being trapped in the proximal basins, flow stripping at the sill is
504 inferred to have occurred, with coarser-grained sediment fractions being trapped in the

upstream basin and with fines predominantly being carried in suspension into the adjacent downslope basin (e.g., Sinclair and Tomasso, 2002). This phenomenon has been illustrated in laboratory and numerical modelling of the interaction of turbidity currents with static structures (Brunt et al., 2004; Lamb et al., 2004, 2006; Nasr-Azadani et al., 2013); however, these simulations cannot directly model the dynamic evolution of deformation, sedimentation and compaction over geological timescales.

In both the documented outcrop and subsurface examples, the lobe complexes are seen to stack aggradationally, producing amalgamated lobe complexes hundreds of metres thick; far in excess of the thicknesses typically documented in unconfined settings (e.g., Fig. 13; Table 3; Prelat et al., 2009; Macdonald et al., 2011; Straub and Pyles, 2012; Cullis et al., 2019). More typically, lobe complexes are seen to be separated by thinner bedded, muddier sediment, either representing a shutdown or an avulsion of the sedimentary system (Prelat et al., 2009). A lateral and vertical transition to finer grained, thinner-bedded strata (LA2) is seen at outcrop (Fig. 9), whilst lower amplitude reflectors (SF1) are seen across the remainder of the basin imaged in the subsurface (Fig. 12A). That these coarse sediments are isolated within a dominantly fine-grained system implies that regional changes in sediment supply along the margin was unlikely responsible for the variation in sediment type (Fig. 2), if such a scenario existed a similar caliber of deposits would be expected all along the margin (Fig. 12A). Although similar thicknesses have been documented for alternations of channel complexes, lobe complexes and MTDs in the northern portion of the Hikurangi Margin (Burgreen and Graham, 2014), those lobe complexes are offset along the trench-slope basin axis rather than aggradationally stacked, consequently with a lower N:G than described in the axial deposits here.

Taking the thickness of the biostratigraphically constrained outcropping lobes at 200 m over an interval of at maximum 2.8 Ma (NZ Altonian stage 18.7 – 15.9 Ma) would give an

minimum average sedimentation rate of ca. 0.71 m / ky. In reality, the timespan over which the lobes were deposited likely represents a much shorter interval as they are truncated by an erosive MTD; the subsurface example also shows truncation by an overlying MTD (Fig. 12). Furthermore, if decompacted using the standard decompation theory of porosity reducing with depth (Sclater and Christie, 1980):

Decompacted sandstone thickness = 172 m * (1-0.25)/(1-0.49) = 253 m

Decompacted mudstone thickness = 28 m * (1-0.2)/(1-0.63) = 60.5 m

This would yield a total decompacted thickness of 313.5 m over 2.8 Ma, giving a decompacted sedimentation rate of at least 1.1 m / ka. This is in excess of the displacement range of thrust faults in the subduction wedge, which range from 0.3 – 0.9 m / ka (Barnes and Nicol, 2004). Therefore, without consideration of an alternative mechanism for generating accomodation, sedimentation would have rapidly filled the structural accomodation, leading to wholescale bypass (e.g., McArthur and McCaffrey, 2019).

## DISCUSSION

### *Controls on repeated stacking of lobes: sediment – structure feedback*

Under bounding conditions of consistent sediment supply, deformation rates and compaction of sediments, three scenarios are plausible:

1) Net sediment aggradation rate > sill uplift rate

This scenario would rapidly result in burial of existing structures and either loss of confinement, as ultimately seen in the subsurface (Fig. 11) or development of a through-going bypass conduit. This is seen in the overlying Middle Miocene interval of the outcropping system (McArthur and McCaffrey, 2019). Here, we do not see immediate

552 erosion of the sill, which would rapidly lead to the development of a spill conduit and
553 wholesale downstream bypass (e.g., Casciano et al., 2019).

554 2) Net sediment aggradation rate < sill uplift rate

555 Growth of bounding structures at rates greater than sediment supply and burial would
556 result in a return to ponded conditions, potentially developing a sheet-like fill across the basin
557 (e.g., Prather et al., 2012; Patacci et al., 2015). This scenario is contrary to the observed
558 variation in sediment distribution and lack of thick mud-caps (Dorrell et al., 2018).

559 3) Net sediment aggradation rate ≈ sill uplift rate

560 In order to sustain the effectively fixed confinement condition required to develop the
561 aggradational lobe complexes described here, a balance between growth of the basin
562 bounding structures and net sedimentation rate is required. Under the scenario in which
563 sedimentation rates and structure growth rates are set independently this condition would
564 seem unlikely to arise frequently; yet here we document multiple instances of aggradationally
565 stacked lobe complexes developed upstream of sills across space and time. Although the
566 development of stacked lobe complexes tens of metres thick trapped in local accommodation
567 has been documented (e.g., Tinterri and Muzzi Magalhaes, 2011; Tinterri and Tagliaferri,
568 2015), these local depocentres are typically rapidly filled by the sediment input, resulting in a
569 migration of the depocentre.

570 Structure growth alone cannot account for the observed stratal thickness, with rates of
571 fault movement in the study area being insufficient to maintain accommodation with high
572 rates of sediment influx (Barnes and Nicol, 2004). Studies have shown that growth of faults
573 and fault related-folds can be intrinsically linked to the sedimentary fill and loading of
574 accommodation (e.g., Noda, 2018; Butler, 2019; Serck and Braathen, 2019). To account for

575 the common development of fixed confinement conditions for extended periods we suggest
576 that a feedback mechanism of sediment – structure interaction may operate (Fig. 14).
577 Initially, sediment ponding in the basin centre was onlapping the basin edges, whilst syn-
578 sedimentary deformation was related to intra-basinal structures (Fig. 14A). This model
579 proposes that sediment loading within the basin eventually results in focusing of stress on the
580 basin bounding faults, with abandonment of the previously active intra-basinal structures as
581 they are buried (Fig. 14B). Continued trapping of coarse sediment behind the growth
582 structure results in sustained sediment loading, coupled with growth of the sill (Fig. 14C-D),
583 permitting the development of vertically stacked lobe complexes hundreds of metres thick.
584 The isostatic loading and focusing of stress on the basin bounding structures may also help to
585 perpetuate tectonic loading in front of the growth structures, further driving generation of
586 accommodation space (Fig. 14D).

587 Ultimately, external forcing (e.g., sediment re-routing, switch-off of sediment supply,
588 progressive outboard migration of deformation, wholescale changes in the style of
589 deformation, or the emplacement of basin-wide MTDs) disrupts the balanced interaction of
590 sedimentation and structuration, resulting in a change in sedimentary style (Fig. 14E). Similar
591 models of sediment load-driven subsidence have been proposed for salt domains (Vendeville,
592 2005), but hitherto have not been explicitly interpreted to operate in fold and thrust belts.
593 Stress modelling of the margin evolution and / or advanced forward modelling of basin
594 structure and fill will help constrain this evolution, but is beyond the scope of this study.

595 These concepts of sedimentation modulating structure growth and hence accommodation
596 raise the potential for similar deposits in other fold and thrust belts. For example Cascadia
597 (Nelson et al., 2000), the deep-water portion of the Makran (Bourget et al., 2011) and
598 offshore Sabah (Jackson et al., 2009).

599 *Allogenic vs autogenic influences on confined lobe complex stacking patterns*

600 An interplay of auto- and allogenic factors is inferred to contribute to the evolution of
601 the aggradational lobe complexes by generating a sill whose relative elevation with respect to
602 the aggrading sediment surface was relatively invariant (Fig. 15). Protracted and repeated
603 flow stripping over this sill, with preferential bypass of fines, i.e. an autogenic control,
604 resulted in the development of aggradationally stacked lobe complexes hundreds of metres
605 thick (Fig. 15A-C). As with lobe complexes observed by Burgreen and Graham (2014) in the
606 northern portion of the Hikurangi Margin, these lobes appear to form very thick,
607 amalgamated complexes, implying that they were likely deposited in tortuous corridors in
608 this convergent setting. However, the interpretation of Burgreen and Graham (2014) that the
609 lobes were migrating along the axis of the trench-slope basin is not applicable in either of the
610 examples documented here. Aggradational lobe complexes described elsewhere cannot
611 compare to the thicknesses observed here (Table 3; Fig. 13). However, the spatial extent of
612 these confined lobe complexes is limited compared to the scale of other documented lobe
613 complexes (Prelat et al., 2010), which may be self-regulating, scaling with size of the
614 generated accomodation. Variability in factors such as turbidity flow thickness, turbidity
615 current frequency and incremental compaction-related subsidence may have influenced
616 individual bed development but are unlikely to have affected the first-order pattern of
617 stratigraphic architecture, which is seen repeatedly in the fill of trench-slope basins on this
618 margin.

619 Overspill of fines into downstream basins may result in the development of thick
620 intervals of turbidite silt- and mudstone there (Fig. 15C). Recognition of this process in the
621 subsurface may be difficult (Volvoikar et al., 2020). Therefore, it may be challenging to
622 distinguish thick intervals of rapidly accumulated turbidite fines from those of slowly

623 accumulated pelagic or hemipelagic sediments, and thus to establish accurate sedimentation
624 rates in trench-slope basin fills (e.g., Boulesteix et al., 2019).

625 In both examples shown here, external forcing is seen to modify the system to the
626 degree that sediment pathways were fundamentally altered (Fig. 15D). Similar effects have
627 been documented in other confined deep-marine settings (e.g., Haughton, 2000; Soutter et al.,
628 2019). The MTD emplacement across the basin may have been related to a wider
629 modification of the margin structure and could also have blocked or diverted the sediment
630 supply or otherwise destabilised the balance of sedimentation and deformation (e.g., Bull et
631 al., 2020). Alteration of the regional stress field (unbalancing the feedback mechanism
632 invoked here or causing structuration that diverted flow pathways) or a significant decrease
633 or increase of the sediment supply could also disrupt the maintenance of a partial-ponding
634 condition, leading to changes in the sedimentary system.

635 *Implications for active margin resource distribution*

636 The aggradational lobe complexes documented here represent the cleanest and
637 thickest development of potentially reservoir-grade sediments within the trench-slope basins,
638 be that for conventional hydrocarbons, as aquifers, or as sites for carbon sequestration.
639 Although unpublished, a similar model of sediment-structure interaction has been invoked to
640 explain the presence of ca. 200 m of stacked sandstones in the Troika Field, Gulf of Mexico.
641 This is also within a system that is overall relatively mud-rich, albeit in a different tectonic
642 setting (Horine et al., 2000). Therefore, our model may help explain the presence of
643 anomalously thick deep-marine sandstones in subsurface examples where deposition
644 occurred in a confined setting (Kirkova-Pourciau and Hill, 2004).

645 In particular, subsequently inverted basins may develop suitable structural closures
646 within which the lobes may be located. Although the lobe complexes are dominantly

aggradational, a minor degree of compensational stacking (Fig. 10) implies they are not entirely as simple as purely vertically stacked reservoir and consideration of variable reservoir properties across different lobe complexes may be anticipated in a vertical section. Abandoned structures underlying the basins may act as fluid pathways to charge intra-basinal lobe complexes (Fig. 10).

Identification of these units in the subsurface may prove difficult, particularly after deformation responsible for trap formation. Therefore, a schematic wireline log signature generated from the outcropping systems may aid exploration in such settings (Fig. 16). Bypass-dominated fine-grained intervals, occurring in discontinuous lenses (Fig. 4A), are not laterally extensive and would not act as barriers to fluid flow. Conversely, the mudstones of the lobe fringe, or those accumulating in downstream basins, would likely be laterally continuous, presenting baffles or barriers to flow.

## CONCLUSIONS

The relationship between deep-marine sedimentation and deformation has been investigated from trench-slope basin fill and structure from the Hikurangi subduction margin, New Zealand. Information from outcropping and subsurface basins on the same margin has been integrated to describe sandstone-rich submarine lobe complexes, aggrading and amalgamated into packages hundreds of meters thick. When possible, the integration of the detailed sedimentology afforded by outcrops with the seismic scale system architecture yields novel insights to the evolution of sedimentary systems and their interaction with growth structures. Here, outcrop studies and seismic data analysis indicate that flow stripping occurred as turbidity currents encountered seafloor structures, resulting in the accumulation of sand-rich deposits behind thrust-cored sills whose thickness implies that a partial ponding condition was maintained for extended periods. Simple scenarios of passive basin infill

671 cannot account for the continued accumulation of these deposits, which reach 300 m in
672 thickness, nor can scenarios with no links between the tectonic rejuvenation of confinement
673 and ongoing sedimentation. Accordingly, a depositional model for sedimentary modulation of
674 tectonic structure growth is proposed in which:

675 • An influx of sediment into confined basins drives isostatic loading and
676 suppresses intrabasinal structure growth, focusing stress onto basin bounding
677 faults.

678 • Activity on basin bounding faults maintains the development of
679 accommodation and relatively fixed, but partial confinement enables the
680 repeated deposition of thick-bedded, clean, amalgamated sandstones, forming
681 aggradational lobe complexes hundreds of metres thick, as finer-grained
682 sediment fractions are stripped and bypassed to deeper basins. This constitutes
683 an autogenic control on the development of lobe complexes.

684 • Eventually allogenic forcing (e.g., regional mass-transport deposit
685 emplacement, upstream modification of feeder pathways, significant changes
686 in the sediment flux and/or the rates of deformation) alters the sedimentary
687 system, such that turbidite lobes no longer form at the same locality.

688 Therefore, sediment flux and loading are inferred to interact with the tectonism,
689 creating a feedback loop, with implications for the tectono-stratigraphic evolution of deep-
690 marine fold and thrust belts. This coupling of sedimentation and deformation may have
691 resulted in the accumulation of thick syn-kinematic turbidite lobe complexes in other
692 confined basins during times of optimally balanced structural evolution and sediment flux.
693 Although amalgamated lobe complexes may be hundreds of meters thick, their areal extent
694 may genetically tie to the wavelength of deformation, hence limiting their areal distribution.

This study effectively permits the inference of a range of conditions under which partial confinement can be maintained. A linkage between sedimentation and deformation is proposed, with sediment input rates high enough to prevent development of full ponding and allowing partial bypass, but not so high as to cause erosion on the sill and complete bypass. Understanding the bounding conditions that lead to such accumulations may help define deep-marine sediment sinks and enhance resource exploration in deep-marine fold and thrust belts.

## ACKNOWLEDGEMENTS

This research was funded by a JIP between Chevron, Equinor, OMV and Schlumberger. WesternGeco Multiclient are thanked for permission to publish seismic data. Hugh Morgans of GNS and the information contained in the New Zealand Fossil Record File are acknowledged for foraminifera biostratigraphy. Land owners are kindly thanked for access to the study area. Many thanks to field assistants Vanisha Pullan and Nick Zajac; Alan Clare, Petter Bjørgen and Frank Chanier for thoughtful insights; David Francis of Geological Research for introduction to the field area and Cécile Robin for helping JuB measure sections. We thank Associated Editor Amy Weislogel and reviewers Katherine Maier and Nora Nieminski for their helpful and constructive reviews.

## REFERENCES

Bailey, W.E., McArthur, A.D., and McCaffrey, W.D., 2020. Distribution of contourite drifts on convergent margins: examples from the Hikurangi subduction margin of NZ. Sedimentology, pp. 55. doi:10.1111/SED.12779

Bailleul, J., Chanier, F., Ferrière, J., Robin, C., Nicol, A., Mahieux, G., Gorini, C., and Caron, V., 2013, Neogene evolution of lower trench-slope basins and wedge development in the

718 central hikurangi subduction margin, new zealand: Tectonophysics, v. 591, p. 152–174,
719 doi: 10.1016/j.tecto.2013.01.003.

720 Bailleul, J., Robin, C., Chanier, F., Guillocheau, F., Field, B., and Ferriere, J., 2007, Turbidite
721 Systems in the Inner Forearc Domain of the Hikurangi Convergent Margin (New
722 Zealand): New Constraints on the Development of Trench-Slope Basins: Journal of
723 Sedimentary Research, v. 77, p. 263–283, doi: 10.2110/jsr.2007.028.

724 Barnes, P.M., and de Lepinay, B.M., 1997, Rates and mechanics of rapid frontal accretion
725 along the very obliquely convergent southern Hikurangi margin , New Zealand: Journal
726 of Geophysical Research, v. 102, p. 24,931-24,952, doi: 10.1029/97JB01384.

727 Barnes, P.M., and Nicol, A., 2004, Formation of an active thrust triangle zone associated with
728 structural inversion in a subduction setting, eastern New Zealand: Tectonics, v. 23.

729 Barnes, P.M., Nicol, A., and Harrison, T., 2002, Late Cenozoic evolution and earthquake
730 potential of an active listric thrust complex above the Hikurangi subduction zone, New
731 Zealand: Geological Society of America Bulletin, v. 114, p. 1379–1405.

732 Barnes, P.M., Lamarche, G., Bialas, J., Henrys, S., Pecher, I., Netzeband, G.L., Greinert, J.,
733 Mountjoy, J.J., Pedley, K., and Crutchley, G., 2010, Tectonic and geological framework
734 for gas hydrates and cold seeps on the Hikurangi subduction margin, New Zealand:
735 Marine Geology, v. 272, p. 26–48, doi: 10.1016/j.margeo.2009.03.012.

736 Barnes, P.M., Ghisetti, F.C., Ellis, S., and Morgan, J.K., 2018, The role of protothrusts in
737 frontal accretion and accommodation of plate convergence, Hikurangi subduction
738 margin, New Zealand: Geosphere, v. 14, p. 440–468, doi: 10.1130/GES01552.1.

739 Beanland, S., Melhuish, A., Nicol, A., and Ravens, J., 1998, Structure and deformational
740 history of the inner forearc region, Hikurangi subduction margin, New Zealand: New

741 Zealand Journal of Geology and Geophysics, v. 41, p. 325–342, doi:
742 10.1080/00288306.1998.9514814.

743 Booth, J.R., Dean, M.C., DuVernay, A.E., and Styzen, M.J., 2003, Paleo-bathymetric
744 controls on the stratigraphic architecture and reservoir development of confined fans in
745 the Auger Basin: central Gulf of Mexico slope: Marine and Petroleum Geology, v. 20, p.
746 563–586, doi: 10.1016/j.marpetgeo.2003.03.008.

747 Boulesteix, K., Poyatos-Moré, M., Flint, S.S., Taylor, K.G., Hodgson, D.M. and Hasiotis,
748 S.T., 2019, Transport and deposition of mud in deep-water environments: Processes and
749 stratigraphic implications: Sedimentology, v. 66, p.2894-2925.

750 Bourget, J., Zaragosi, S., Mulder, T., Schneider, J.L., Garlan, T., Van Toer, A., Mas, V., and
751 Ellouz-Zimmermann, N., 2010, Hyperpycnal-fed turbidite lobe architecture and recent
752 sedimentary processes: A case study from the Al Batha turbidite system, Oman margin:
753 Sedimentary Geology, v. 229, p. 144-159.

754 Bourget, J., Zaragosi, S., Ellouz-Zimmermann, N., Mouchot, N., Garlan, T., Schneider, J.L.,
755 Lanfumey, V. and Lallemant, S., 2011, Turbidite system architecture and sedimentary
756 processes along topographically complex slopes: the Makran convergent
757 margin: Sedimentology, v. 58, p.376-406.

758 Braaksma, H, Kenter, J.A.M., Proust, J.N., Z, Dijkmans, V., Van Hoek, T, Mahieux, G. and
759 Drijkoningen, G.G., 2003, Controls on acoustic properties of Upper Jurassic siliciclastic
760 rocks (Boulonnais, northern France): Geophysics, v. 68, p. 58-69.

761 Brunt, R.L., McAffrey, W.D., and Kneller, B.C., 2004, Experimental modeling of the spatial
762 distribution of grain size developed in a fill-and-spill mini-basin setting: Journal of
763 Sedimentary Research, v. 74, p. 438–446.

764 Brunt, R.L., Hodgson, D.M., Flint, S.S., Pringle, J.K., Di Celma, C., Prélat, A., and Grecula,
765 M., 2013, Confined to unconfined: Anatomy of a base of slope succession, Karoo Basin,
766 South Africa: Marine and Petroleum Geology, v. 41, doi:
767 10.1016/j.marpetgeo.2012.02.007.

768 Burgess, P. M., Masiero, I., Toby, S. C. and Duller, R. A., 2019,. A Big Fan of Signals?
769 Exploring Autogenic and Allogenic Process and Product In a Numerical Stratigraphic
770 Forward Model of Submarine-Fan Development: Journal of Sedimentary Research v.
771 89, p. 1-12.

772 Burgreen, B., and Graham, S., 2014, Evolution of a deep-water lobe system in the Neogene
773 trench-slope setting of the East Coast Basin, New Zealand: Lobe stratigraphy and
774 architecture in a weakly confined basin configuration: Marine and Petroleum Geology,
775 v. 54, p. 1–22, doi: 10.1016/j.marpetgeo.2014.02.011.

776 Burgreen-Chan, B., Meisling, K.E., and Graham, S., 2016, Basin and petroleum system
777 modelling of the East Coast Basin, New Zealand: a test of overpressure scenarios in a
778 convergent margin: Basin Research, v. 28, p. 536–567, doi: 10.1111/bre.12121.

779 Bull, S., Browne, G.H., Arnot, M.J. and Strachan, L.J., 2020, Influence of mass transport
780 deposit (MTD) surface topography on deep-water deposition: an example from a
781 predominantly fine-grained continental margin, New Zealand. Geological Society,
782 London, Special Publications, v. 500, pp. 25.

783 Butler, R.W.H., 2019, Syn-kinematic strata influence the structural evolution of emergent
784 fold-thrust belts: Geological Society, London, Special Publications, v. 490, p. SP490--
785 2019.

786 Casciano, C. I., Patacci, M., Longhitano, S. G., Tropeano, M., McCaffrey, W. D. and Di

787 Celma, C., 2019, Multi-scale analysis of a migrating submarine channel system in a
788 tectonically-confined basin: The Miocene Gorgoglione Flysch Formation, southern
789 Italy: Sedimentology v. 66, p. 205-240.

790 Chanier, F., and Ferriere, J., 1991, From a passive to an active margin; tectonic and
791 sedimentary processes linked to the birth of an accretionary prism (Hikurangi Margin,
792 New Zealand): Bulletin de la Société géologique de France, v. 162, p. 649–660.

793 Chanier, F., Ferrière, J., and Angelier, J., 1999, Extensional deformation across an active
794 margin, relations with subsidence, uplift, and rotations: The Hikurangi subduction, New
795 Zealand: Tectonics, v. 18, p. 862–876, doi: 10.1029/1999TC900028.

796 Clift, P., Gaedicke, C., Edwards, R., Lee, J. Il, Hildebrand, P., Amjad, S., White, R.S., and
797 Schlüter, H.-U., 2002, The stratigraphic evolution of the Indus Fan and the history of
798 sedimentation in the Arabian Sea: Marine Geophysical Researches, v. 23, p. 223–245.

799 Cohen, K.M., Finney, S.C., Gibbard, P.L., and Fan, J.-X., 2013, The ICS international
800 chronostratigraphic chart: Episodes, v. 36, p. 199–204.

801 Covault, J.A., Normark, W.R., Romans, B.W., and Graham, S.A., 2007, Highstand fans in the
802 California borderland: The overlooked deep-water depositional systems: Geology, v.35,
803 p. 783–786.

804 Crisostomo Figueroa, A., McArthur, A.D., Dorrel, R., Amy, L., and McCaffrey, W.D., 2020,
805 A new modelling approach to sediment bypass prediction applied to the East Coast
806 Basin, New Zealand: Geological Society of America Bulletin, pp. 15,
807 https://doi.org/10.1130/B35687.1

808 Cullis, S., Patacci, M., Colombera, L., Bührig, L. and McCaffrey, W.D., 2019, A database
809 solution for the quantitative characterisation and comparison of deep-marine siliciclastic

depositional systems: Marine and Petroleum Geology, v. 102, p.321-339.

Dennielou, B., Droz, L., Babonneau, N., Jacq, C., Bonnel, C., Picot, M., Le Saout, M., Saout, Y., Bez, M., Savoye, B. and Olu, K., 2017, Morphology, structure, composition and build-up processes of the active channel-mouth lobe complex of the Congo deep-sea fan with inputs from remotely operated underwater vehicle (ROV) multibeam and video surveys: Deep Sea Research Part II: Topical Studies in Oceanography, v. 142, p.25-49.

Deptuck, M.E., Piper, D.J.W., Savoye, B., and Gervais, A., 2008, Dimensions and architecture of late Pleistocene submarine lobes off the northern margin of East Corsica: Sedimentology, v. 55, p. 869–898.

Dorrell, R. M., Patacci, M., and McCaffrey, W. D., 2018, Inflation of Ponded, Particulate Laden Density Currents: Journal of Sedimentary Research, v.88, p.1276-1282.

Etienne, S., Mulder, T., Bez, M., Desaubliaux, G., Kwasniewski, A., Parize, O., Dujoncquoy, E., and Salles, T., 2012, Multiple scale characterization of sand-rich distal lobe deposit variability: examples from the Annot Sandstones Formation, Eocene--Oligocene, SE France: Sedimentary Geology, v. 273, p. 1–18.

Figueiredo, J.J.P., Hodgson, D.M., Flint, S.S., and Kavanagh, J.P., 2010, Depositional environments and sequence stratigraphy of an exhumed Permian mudstone-dominated submarine slope succession, Karoo Basin, South Africa: Journal of Sedimentary Research, v. 80, p. 97-118.

Figueiredo, J.J.P., Hodgson, D.M., Flint, S.S., and Kavanagh, J.P., 2013, Architecture of a channel complex formed and filled during long-term degradation and entrenchment on the upper submarine slope, Unit F, Fort Brown Fm., SW Karoo Basin, South Africa: Marine And Petroleum Geology, v. 41, p. 104-116.

833 Flint S.S., Hodgson, D.M., Sprague, A.R., Brunt, R.L., van der Merwe, W.C., Figueiredo
834 J.J.P., Prelat A., Box D., Di Celma C.N., and Kavanagh J.P., 2011, Depositional
835 architecture and sequence stratigraphy of the Karoo basin floor to shelf edge succession,
836 Laingsburg depocentre, South Africa: Marine And Petroleum Geology, v.28, p. 658-674.

837 Flood, R.D., Manley, P.L., Kowsmann, R.O., Appi, C.J., and Pirmez, C., 1991, Seismic
838 facies and late Quaternary growth of Amazon submarine fan, in Weimer, P., and Link,
839 M.H., eds., Seismic facies and sedimentary processes of submarine fans and turbidite
840 systems., New York, NY, United States, Springer-Verlag, p. 415-433.

841 Francis, D.A., and Johansen, A., 2011, Geology of the Kawakawa Structure: Ministry of
842 Economic Development New Zealand, Petroleum Report Series PR4482, 48 p.

843 Grecula, M., Flint, S.S., Wickens, H. d.V., and Johnson, S.D., 2003 Upward-thickening
844 patterns and lateral continuity of Permian sand-rich turbidite channel fills, Laingsburg
845 Karoo, South Africa: Sedimentology, v. 50, p. 831-853.

846 Grundvag, S.-A., Johannessen, E.P., Helland-Hansen, W., Plink-Bjoerklund, P., 2014,
847 Depositional architecture and evolution of progradationally stacked lobe complexes in
848 the Eocene Central Basin of Spitsbergen: Sedimentology, v.61, p. 535-569.

849 Haughton, P.D.W., 2000, Evolving turbidite systems on a deforming basin floor, Tabernas,
850 SE Spain: Sedimentology, v. 47, p. 497–518.

851 Haughton, P.D., Barker, S.P. and McCaffrey, W.D., 2003, 'Linked'debrites in sand-rich
852 turbidite systems–origin and significance: Sedimentology, v. 50, p.459-482.

853 Heron, D.W. (custodian), 2014, Geological map of New Zealand 1:250,000. Lower Hutt,
854 NZ: GNS Science. GNS Science geological map 1. 1 CD.

855 Hofstra, M., Hodgson, D.M., Peakall, J., and Flint, S.S., 2015, Giant scour-fills in ancient
856 channel-lobe transition zones: Formative processes and depositional architecture:
857 Sedimentary Geology, v. 329, p. 98-114.

858 Horine, R.L., Mills, W.H., Sturrock, V.J., and Anthony, M., 2000, Structural controls on
859 sedimentation and hydrocarbon charge in the Troika Field—deepwater Gulf of Mexico
860 (abstract): American Association of Petroleum Geologists, 2000 Annual Meeting,
861 Abstract Volume, p. A69.

862 Jackson, C.A.L., Zakaria, A.A., Johnson, H.D., Tongkul, F., and Crevello, P.D., 2009,
863 Sedimentology, stratigraphic occurrence and origin of linked debrites in the West
864 Crocker Formation (Oligo-Miocene), Sabah, NW Borneo: Marine and Petroleum
865 Geology, v. 26, p.1957-1973.

866 Jegou, I., Savoye, B., Pirmez, C., and Droz, L., 2008, Channel-mouth lobe complex of the
867 recent Amazon Fan: the missing piece: Marine Geology, v. 252, p. 62–77.

868 Jiao, R., Seward, D., Little, T.A., and Kohn, B.P., 2015, Unroofing of fore-arc ranges along
869 the Hikurangi Margin, New Zealand: Constraints from low-temperature
870 thermochronology: Tectonophysics, v. 656, p.39-51.

871 Joseph, P., Babonneau, N., Bourgeois, A., Cotteret, G., Eschard, R., Garin, B., Gomes De
872 Souza, O., Granjeon, D., Guillocheau, F., Lerat, O., and Quemener, J.M., 2000: The
873 Annot Sandstone outcrops (French Alps): architecture description as input for
874 quantification and 3D reservoir modeling, *in* Weimer, P., ed., Deep-Water Reservoirs of
875 the World: Gulf Coast Section SEPM Foundation 20th Annual Research Conference,
876 SEPM Special Publication, V. 28, p. 422-449.

877 Jobe, Z.R., Sylvester, Z., Howes, N., Pirmez, C., Parker, A., Cantelli, A., Smith, R.,

878 Wolinsky, M.A., O'Byrne, C., Slowey, N., and Prather, B., 2017, High-resolution,
879 millennial-scale patterns of bed compensation on a sand-rich intraslope submarine fan,
880 western Niger Delta slope: Geological Society of America Bulletin, v. 129, p. 23-37.

881 Jobe, Z.R., Howes, N., Romans, B.W., Covault, J.A., 2018, Volume and recurrence of
882 submarine-fan-building turbidity currents: Depositional Record, v. 4, p. 160-176.

883 Kane, I.A., McCaffrey, W.D., and Martinsen, O.J., 2009, Allogenic vs. autogenic controls on
884 megaflute formation: Journal of Sedimentary Research, v. 79, p.643-651.

885 Kane, I.A., Pontén, A.S.M., Vangdal, B., Eggenhuisen, J.T., Hodgson, D.M., and Spychala,
886 Y.T., 2017, The stratigraphic record and processes of turbidity current transformation
887 across deep-marine lobes: Sedimentology, v. 64, p. 1236-1273.

888 Kirkova-Pourciau, J.T., and Hill, W.A., 2004, Seismic Facies Mapping on the Major
889 Reservoir Producer (S10) in the Troika Field: Gulf Coast Association of Geological
890 Societies Transactions, v. 54, p. 305-312.

891 Kneller, B. and McCaffrey, W., 1999, Depositional effects of flow nonuniformity and
892 stratification within turbidity currents approaching a bounding slope; deflection,
893 reflection, and facies variation: Journal of Sedimentary Research, v. 69, p.980-991.

894 Iorio, M., Liddicoat, J.C., Budillon, F., Tiano, P., Incoronato, A., Coe, R.S., and Marsella, E.,
895 2009, Paleomagnetic secular variation time constraints on late Neogen geological events
896 in slope sediment from the eastern Tyrrhenian Sea, *in* Kneller, B.C., Martinsen, O.J., and
897 McCaffrey, W.D., eds. External Controls on Deep-Water Depositional Systems: Society
898 for Sedimentary Geology, Special Publication v. 92, p. 233-243.

899 Lamb, M.P., Hickson, T., Marr, J.G., Sheets, B., Paola, C., and Parker, G., 2004, Surging
900 versus continuous turbidity currents: flow dynamics and deposits in an experimental

intraslope minibasin: Journal of Sedimentary Research, v. 74, p. 148–155.

Lamb, M.P., Toniolo, H., and Parker, G., 2006, Trapping of sustained turbidity currents by intraslope minibasins: Sedimentology, v. 53, p. 147–160.

Lee, J.M. and Begg, J.G., 2002, Geology of the Wairarapa area: Institute of Geological & Nuclear Sciences 1:250,000 geological map 11. 1 sheet + 66 pages. Institute of Geological and Nuclear Sciences Ltd, Lower Hutt, New Zealand.

Lericolais, G., Bourget, J., Popescu, I., Jermannaud, P., Mulder, T., Jorry, S., and Panin, N., 2013, Late Quaternary deep-sea sedimentation in the western Black Sea: New insights from recent coring and seismic data in the deep basin: Global and Planetary Change, v. 103, p. 232-247.

Lewis, K.B., and Pettinga, J.R., 1993, The emerging, imbricate frontal wedge of the Hikurangi margin: Sedimentary basins of the world, v. 2, p. 225–250.

Lillie, A.R., 1953, The geology of the Dannevirke Subdivision: New Zealand Geological Survey bulletin, v. 46, 156 p.

Litchfield, N., Ellis, S., Berryman, K., and Nicol, A., 2007, Insights into subduction-related uplift along the Hikurangi Margin, New Zealand, using numerical modeling: Journal of Geophysical Research: Earth Surface, v. 112, p. 1–17, doi: 10.1029/2006JF000535.

Liu, Q., Kneller, B.C., Fallgatter, C., and Buso, V.V., 2018, Quantitative comparisons of depositional architectures of unconfined and confined turbidite sheet systems: Sedimentary Geology, v. 376, p. 72-89.

Macdonald, H.A., Peakall, J., Wignall, P.B., and Best, J., 2011, Sedimentation in deep-sea lobe-elements: implications for the origin of thickening-upward sequences: Journal of

the Geological Society, v. 168, p. 319–332.

Maier, K.L., Paull, C.K., Caress, D.W., Anderson, K., Nieminski, N.M., Lundsten, E., Erwin, B.E., Gwiazda, R., and Fildani, A., 2020, Submarine-fan development revealed by integrated high-resolution datasets from La Jolla Fan, offshore California, USA: Journal of Sedimentary Research, v. 90, p.468-479.

Malié, P., Bailleul, J., Chanier, F., Toullec, R., Mahieux, G., Caron, V., Field, B., Mählmann, R.F., and Potel, S., 2017, Spatial distribution and tectonic framework of fossil tubular concretions as onshore analogues of cold seep plumbing systems, North Island of New Zealand. Bulletin de la Société géologique de France, v. 188, pp. 25.

Marini, M., Milli, S., Ravnas, R., and Moscatelli, M., 2015, A comparative study of confined vs. semi-confined turbidite lobes from the Lower Messinian Laga Basin (Central Apennines, Italy): Implications for assessment of reservoir architecture: Marine and Petroleum Geology, v.63, p.142-165.

Marini, M., Patacci, M., Felletti, F., and McCaffrey, W.D., 2016a, Fill to spill stratigraphic evolution of a confined turbidite mini-basin succession, and its likely well bore expression: The Castagnola Fm, NW Italy: Marine and Petroleum Geology, v. 69, p. 94–111.

Marini, M., Felletti, F., Milli, S., and Patacci, M., 2016b, The thick-bedded tail of turbidite thickness distribution as a proxy for flow confinement: Examples from tertiary basins of central and northern Apennines (Italy): Sedimentary Geology, v.341, p.96-118.

Maselli, V., Kneller, B., Taiwo, O.L., and Iacopini, D., 2019, Sea floor bedforms and their influence on slope accommodation: Marine and Petroleum Geology, v. 102, p. 625–637.

Mayall, M., and Stewart, I., 2000, The Architecture of Turbidite Slope Channels, *in* Deep-

946 Water Reservoirs of the World: 20th Annual, Society of Economic Paleontologists and
947 Mineralogists, v. Deep-Water, p. 578–586, doi: 10.5724/gcs.00.15.0578.

948 Mayall, M., Lonergan, L., Bowman, A., James, S., Mills, K., Primmer, T., Pope, D., Rogers,
949 L. and Skeene, R., 2010, The response of turbidite slope channels to growthinduced
950 seabed topography: AAPG Bulletin, v.94, p.1011–1030.

951 McArthur, A.D., and McCaffrey, W.D., 2019, Sedimentary architecture of detached deep-
952 marine canyons: Examples from the East Coast Basin of New Zealand: Sedimentology,
953 v. 66, p. 1067–1101.

954 McArthur, A.D., Claussmann, B., Bailleul, J., McCaffrey, W., and Clare, A., 2019, Variation
955 in syn-subduction sedimentation patterns from inner to outer portions of deep-water fold
956 and thrust belts: examples from the Hikurangi subduction margin of New Zealand:
957 Geological Society, London, Special Publications, v. 490, p. SP490--2018.

958 der Merwe, W.C., Hodgson, D.M., Brunt, R.L., and Flint, S.S., 2014, Depositional
959 architecture of sand-attached and sand-detached channel-lobe transition zones on an
960 exhumed stepped slope mapped over a 2500 km2 area: Geosphere, v. 10, p. 1076–1093.

961 Mountjoy, J.J., and Micallef, A., 2012, Polyphase emplacement of a 30 km3 blocky debris
962 avalanche and its role in slope-gully development, *in* Submarine Mass Movements and
963 Their Consequences, Springer, p. 213–222.

964 Nasr-Azadani, M.M., Hall, B., and Meiburg, E., 2013, Polydisperse turbidity currents
965 propagating over complex topography: comparison of experimental and depth-resolved
966 simulation results: Computers & Geosciences, v. 53, p. 141–153.

967 Neef, G., 1992, Turbidite deposition in five miocene, bathyal formations along an active plate
968 margin, North Island, New Zealand: with notes on styles of deposition at the margins of

969 east coast bathyal basins: Sedimentary Geology, v. 78, p. 111–136, doi: 10.1016/0037-
970 0738(92)90116-9.

971 Nelson, C.H., Goldfinger, C., Johnson, J.E. and Dunhill, G., 2000, Variation of modern
972 turbidite systems along the subduction zone margin of Cascadia Basin and implications
973 for turbidite reservoir beds, *in* Weimer, P., ed., Deep-Water Reservoirs of the World:
974 20th Annual Research Conference, Gulf Coast Section Society of Economic
975 Paleontologists and Mineralogists, p. 714 – 738.

976 Nicol, A., and Beavan, J., 2003, Shortening of an overriding plate and its implications for slip
977 on a subduction thrust, central Hikurangi Margin, New Zealand: Tectonics, v. 22.

978 Nicol, A., and Wallace, L.M., 2007, Temporal stability of deformation rates: Comparison of
979 geological and geodetic observations, Hikurangi subduction margin, New Zealand:
980 Earth and Planetary Science Letters, v. 258, p. 397–413, doi:
981 10.1016/j.epsl.2007.03.039.

982 Nicol, A., VanDissen, R., Vella, P., Alloway, B., and Melhuish, A., 2002, Growth of
983 contractional structures during the last 10 m.y. at the southern end of the emergent
984 Hikurangi forearc basin, New Zealand: New Zealand Journal of Geology and
985 Geophysics, v. 45, p. 365–385, doi: 10.1080/00288306.2002.9514979.

986 Nicol, A., Mazengarb, C., Chanier, F., Rait, G., Uruski, C., and Wallace, L., 2007, Tectonic
987 evolution of the active Hikurangi subduction margin, New Zealand, since the Oligocene:
988 Tectonics, v. 26, p. 1–24, doi: 10.1029/2006TC002090.

989 Noda, A., 2018, Forearc basin stratigraphy and interactions with accretionary wedge growth
990 according to the critical taper concept: Tectonics, v. 37, p. 965–988.

991 Normark, W.R., 1978, Fan Valleys, channels, and depositional lobes on modern submarine

992 fans; characters for recognition of sandy turbidite environments: AAPG Bulletin , v. 62,
993 p. 912–931.

994 Normark, W.R., Piper, D.J.W. and Hess, G.R., 1979, Distributary channels, sand lobes, and
995 mesotopography of Navy submarine fan, California Borderland, with applications to
996 ancient fan sediments: Sedimentology, v. 26, p.749-774.

997 Normark, W.R., Piper, D.J.W., and Stow, D.A. V, 1983, Quaternary development of
998 channels, levees, and lobes on middle Laurentian Fan: AAPG Bulletin, v. 67, p. 1400–
999 1409.

1000 Ortiz-Karpf, A., Hodgson, D.M. and McCaffrey, W.D., 2015, The role of mass-transport
1001 complexes in controlling channel avulsion and the subsequent sediment dispersal
1002 patterns on an active margin: the Magdalena Fan, offshore Colombia: Marine and
1003 Petroleum Geology, v.64, p.58-75.

1004 Patacci, M., Haughton, P.D.W., and Mccaffrey, W.D., 2015, Flow behavior of ponded
1005 turbidity currents: Journal of Sedimentary Research, v. 85, p. 885–902.

1006 Picot, M., Droz, L., Marsset, T., Dennielou, B., and Bez, M., 2016, Controls on turbidite
1007 sedimentation: insights from a quantitative approach of submarine channel and lobe
1008 architecture (Late Quaternary Congo Fan): Marine and Petroleum Geology, v. 72, p.
1009 423–446.

1010 Piper, D.J.W., and Normark, W.R., 2001, Sandy fans; from Amazon to Hueneme and
1011 beyond: AAPG Bulletin, v.85, p. 1407-1438.

1012 Pirmez, C., Beaubouef, R.T., Friedmann, S.J., and Mohrig, D.C., 2000, Equilibrium Profile
1013 and Baselevel in Submarine Channels: Examples from Late Pleistocene Systems and
1014 Implications for the Architecture of Deepwater Reservoirs, *in* Weimer, P., ed., Deep-

Water Reservoirs of the World: 20th Annual Research Conference, Gulf Coast Section Society of Economic Paleontologists and Mineralogists, p. 782-805.

Popescu, I., Lericolais, G., Panin, N., Wong, H.K., and Droz, L., 2001, Late Quaternary channel avulsions on the Danube deep-sea fan, Black Sea: Marine Geology, v. 179, p. 25-37.

Posamentier, H.W. and Kolla, V., 2003, Seismic geomorphology and stratigraphy of depositional deepwater deposits: Journal of Sedimentary Research, v.73, p.367–388.

Postma, G., and Kleverlaan, K., 2018, Supercritical flows and their control on the architecture and facies of small-radius sand-rich fan lobes: Sedimentary Geology, v. 364, p. 53-70.

Prather, B.E., 2003, Controls on reservoir distribution, architecture and stratigraphic trapping in slope settings: Marine and Petroleum Geology, v. 20, p. 529–545.

Prather, B.E., Booth, J.R., Steffens, G.S., and Craig, P.A., 1998, Classification, lithologic calibration, and stratigraphic succession of seismic facies of intraslope basins, deep-water Gulf of Mexico: AAPG bulletin, v. 82, p. 701–728.

Prather, B.E., Pirmez, C., and Winker, C.D., 2012, Stratigraphy of linked intraslope basins: Brazos-Trinity system western Gulf of Mexico: Application of the Principles of Seismic Geomorphology to Continental-Slope and Base-of-Slope Systems: Case Studies from Seafloor and Near-Seafloor Analogues: SEPM, Special Publication, v. 99, p. 83–110.

Prelat, A., and Hodgson, D.M., 2013, The full range of turbidite bed thickness patterns in submarine lobes: controls and implications: Geological Society of London, Journal, v. 170, p. 209–214.

Prelat, A., Hodgson, D.M., and Flint, S.S., 2009, Evolution, architecture and hierarchy of

1037 distributary deep-water deposits: a high-resolution outcrop investigation from the
1038 Permian Karoo Basin, South Africa: Sedimentology, v. 56, p. 2132–2154, doi:
1039 10.1111/j.1365-3091.2009.01073.x.

1040 Prelat, A., Covault, J.A., Hodgson, D.M., Fildani, A., and Flint, S.S., 2010, Intrinsic controls
1041 on the range of volumes, morphologies, and dimensions of submarine lobes:
1042 Sedimentary Geology, v. 232, p. 66–76.

1043 Pringle, J.K., Brunt R.L., Hodgson, D.M., and Flint, S.S., 2010, Capturing stratigraphic and
1044 sedimentological complexity from submarine channel complex outcrops to digital 3D
1045 models, Karoo Basin, South Africa: Petroleum Geoscience, v. 16, p. 307-330.

1046 Pyles, D.R., Fleming, A.E.P., and Anderson, D.S., 2019, Hierarchical Organization and
1047 Spatial Variations of Lobes in Distributive Submarine Fans: Outcrop Study of the Point
1048 Loma Formation, California, USA, *in* Marsaglia, K.M., Schwalbach, J.R., and Behl,
1049 R.J., eds., From the Mountains to the Abyss: The California Borderland as an Archive of
1050 Southern California Geologic Evolution. SEPM Special Publication, v. 110, p. 135-157.

1051 Rabouille, C., Dennielou, B., Baudin, F., Raimonet, M., Droz, L., Khripounoff, A., Martinez,
1052 P., Mejanelle, L., Michalopoulos, P., Pastor, L., and Pruski, A., 2019, Carbon and silica
1053 megasink in deep-sea sediments of the Congo terminal lobes: Quaternary Science
1054 Reviews, v. 222, p.105854.

1055 Raine, J.I., Beu, A.G., Boyes, A.F., Campbell, H., Cooper, R.A., Crampton, J.S., Crundwell,
1056 M.P., Hollis, C.J., and Morgans, H.E.G., 2015, Revised calibration of the New Zealand
1057 Geological Timescale: NTGT2015/1: GNS Science Lower Hutt.

1058 Rait, G., Chanier, F., and Waters, D.W., 1991, Landward- and seaward-directed thrusting
1059 accompanying the onset of subduction beneath New Zealand: Geology, v. 19, p. 230–

233, doi: 10.1130/0091-7613(1991)019<0230:LASDTA>2.3.CO;2.

Reyners, M., 2013, The central role of the Hikurangi Plateau in the Cenozoic tectonics of New Zealand and the Southwest Pacific: Earth and Planetary Science Letters, v. 361, p. 460–468, doi: 10.1016/j.epsl.2012.11.010.

Reyners, M., Eberhart-Phillips, D., and Bannister, S., 2011, Tracking repeated subduction of the Hikurangi Plateau beneath New Zealand: Earth and Planetary Science Letters, v. 311, p. 165–171, doi: 10.1016/j.epsl.2011.09.011.

Saller, A., Werner, K., Sugiaman, F., Cebastiant, A., May, R., Glenn, D., and Barker, C., 2008, Characteristics of Pleistocene deep-water fan lobes and their application to an upper Miocene reservoir model, offshore East Kalimantan, Indonesia: AAPG Bulletin, v. 92, p. 919–949, doi: 10.1306/03310807110.

Savoye, B., Babonneau, N., Dennielou, B., and Bez, M., 2009, Geological overview of the Angola-Congo margin, the Congo deep-sea fan and its submarine valleys, *in* Deep Sea Research Part II: Topical studies in Oceanography, v. 56, p. 2169–2182.

Sclater, J.G., and Christie, P.A.F., 1980, Continental stretching: An explanation of the post-Mid-Cretaceous subsidence of the central North Sea Basin: Journal of Geophysical Research: Solid Earth, v. 85, p. 3711–3739.

Serck, S.C., and Braathen, A., 2019, Extensional fault and fold growth: Impact on accommodation evolution and sedimentary infill: Basin Research, v. 31, p. 967–990.

Sinclair, H.D., and Tomasso, M., 2002, Depositional evolution of confined turbidite basins: Journal of Sedimentary Research, v. 72, p. 451–456.

Sixsmith, P.J., Flint, S.S., Wickens, H. d.V., and Johnson, S.D., 2004, Anatomy and

stratigraphic development of a basin floor turbidite system in the Laingsburg Formation, Main Karoo Basin, South Africa: Journal of Sedimentary Research, v. 74, p. 239-254.

Slatt, R.M., Jordan, D.W., D'Agostino, A., and Gillespie, R.H., 1992, Outcrop gamma-ray logging to improve understanding of subsurface well log correlations, *in*: Hurst, A., Griffiths, C.M., Worthington, P.F. (Eds.), Geological Applications of Wireline Logs II. Geological Society, London, Special Publications. v. 65, p. 3–19.

Soutter, E.L., Kane, I.A., Fuhrmann, A., Cumberpatch, Z.A., and Huuse, M., 2019, The stratigraphic evolution of onlap in siliciclastic deep-water systems: Autogenic modulation of allogenic signals: Journal of Sedimentary Research, v. 89, p. 890–917.

Spychala, Y.T., Hodgson, D.M., Flint, S.S., and Mountney, N.P., 2015, Constraining the sedimentology and stratigraphy of submarine intraslope lobe deposits using exhumed examples from the Karoo Basin, South Africa: Sedimentary Geology, v. 322, doi: 10.1016/j.sedgeo.2015.03.013.

Spychala, Y.T., Hodgson, D.M., Prélat, A., Kane, I.A., Flint, S.S., and Mountney, N.P., 2017, Frontal and lateral submarine lobe fringes: comparing sedimentary facies, architecture and flow processes: Journal of Sedimentary Research, v. 87, p. 75–96.

Stevenson, C.J., Jackson, C.A.L., Hodgson, D.M., Hubbard, S.M. and Eggenhuisen, J.T., 2015, Deep-water sediment bypass: Journal of Sedimentary Research, v. 85, p.1058-1081.

Stow, D.A. V, and Johansson, M., 2000, Deep-water massive sands: nature, origin and hydrocarbon implications: Marine and Petroleum Geology, v. 17, p. 145–174.

Straub, K.M., and Pyles, D.R., 2012, Quantifying the hierarchical organization of compensation in submarine fans using surface statistics: Journal of Sedimentary

Research, v. 82, p. 889–898.

Strogen, D.P., Bland, K.J., Nicol, A., and King, P.R., 2014, Paleogeography of the Taranaki Basin region during the latest Eocene–Early Miocene and implications for the "total drowning" of Zealandia: New Zealand Journal of Geology and Geophysics, v. 57, p. 110–127, doi: 10.1080/00288306.2014.901231.

Tinterri, R., and Muzzi Magalhaes, P., 2011, Synsedimentary structural control on foredeep turbidites: An example from Miocene Marnoso-arenacea Formation, Northern Apennines, Italy: Marine and Petroleum Geology, v. 28, p. 629–657, doi: 10.1016/j.marpetgeo.2010.07.007.

Tinterri, R., and Tagliaferri, A., 2015, The syntectonic evolution of foredeep turbidites related to basin segmentation: Facies response to the increase in tectonic confinement (Marnoso-arenacea Formation, Miocene, Northern Apennines, Italy): Marine and Petroleum Geology, v. 67, p. 81–110.

Tinterri, R., and Piazza, A., 2019, Turbidites facies response to the morphological confinement of a foredeep (Cervarola Sandstones Formation, Miocene, northern Apennines, Italy): Sedimentology, v. 66, p. 636–674.

Van Lente, B., 2004, Chemostratigraphic trends and provenance of the Permian Tanqua and Laingsburg depocentres, southwestern Karoo basin, South Africa (Doctoral dissertation, Stellenbosch: University of Stellenbosch). pp. 339.

Vendeville, B.C., 2005, Salt tectonics driven by sediment progradation: Part I—Mechanics and kinematics: AAPG bulletin, v. 89, p. 1071–1079.

Vinnels, J.S., Butler, R.W.H., McCaffrey, W.D. and Paton, D.A., 2010, Depositional processes across the Sinu accretionary prism, offshore Colombia: Marine and Petroleum

Geology, v.27, p.794–809.

Volvoikar, S., Mazumdar, A., Peketi, A., Dewangan, P., Sawant, B., Manaskanya, A., Goswami, H., Das, D. and Pujari, S., 2020, Contrasting sulfidization in the turbidite and hemipelagic sediments of Bengal Fan: Marine and Petroleum Geology, v. 118, 104408.

Wells, P., 1989, Burial history of Late Neogene sedimentary basins on part of the New Zealand convergent plate margin: Basin Research, v. 2, p. 145–160, doi: 10.1111/j.1365-2117.1989.tb00032.x.

Yang, S.-Y., and Kim, J.W., 2014, Pliocene basin-floor fan sedimentation in the Bay of Bengal (offshore northwest Myanmar): Marine And Petroleum Geology, v. 49, p. 45-58.

Zhang, J.J., Wu, S.H., Fan, T.E., Fan, H.J., Jiang, L., Chen, C., Wu, Q.Y., and Lin, P., 2016, Research on the architecture of submarine-fan lobes in the Niger Delta Basin, offshore West Africa: Journal of Palaeogeography, v. 5, p. 185-204.

FIGURE CAPTIONS

Fig. 1. A) Geological map (Heron, 2014) and 400 m grid resolution hillshade bathymetry map (courtesy of NIWA) of the southern portion of the Hikurangi subduction margin. Seismic study focused on area around the MC - Madden Channel; PT - Porangahau Trough; and PR - Porangahau Ridge. B) Schematic cross-section of the Hikurangi subduction complex, after Nicol et al. (2007).

Fig. 2. Schematic chronostratigraphic chart for the southern part of the Hikurangi subduction margin, general section line illustrated on inset map. Regional tectonism adapted from Chanier et al. (1999); Bailleul et al., (2013); Reyners (2013) and Burgreen-Chan et al. (2016).

1150 International time scale after Cohen et al. (2013), New Zealand stages after Raine et al.
1151 (2015). Study intervals highlighted with dashed yellow boxes.

1152

1153 Fig. 3. A) Geological map of the onshore study area in the Akitio Basin (Heron, 2014), with
1154 mapped extent of the lobe complexes and the overlying mass-transport deposits (MTD)
1155 overlain on a shaded relief basemap. B) Cross-section of the Akitio Basin and adjacent
1156 structures; base of the studied Lower Miocene interval indicated with a dashed line. Modified
1157 from Lee and Begg (2002) and Malié et al. (2017). Note the simplified colours shown on the
1158 cross-section are representative of the general stratigraphy, as with Figure 1.

1159

1160 Fig. 4. A) Photo-mosaic of Owahanga Gorge northern side outcrop showing mostly
1161 amalgamated medium to thick-bedded sandstones (LF1), with subordinate laterally
1162 discontinuous thin-beds (LF3) of lithofacies association 1 (LA1). B) Close-up photograph of
1163 the laterally discontinuous thin-beds (LF3), hammer handle for scale is 20 cm long. C) Close-
1164 up photograph of thick-bedded, amalgamated sandstones (LF1). D) Photograph of incisional
1165 cuts and fills interpreted as a distributary channel fill (LF2). E) Logged section through a
1166 distributary channel or scour fill (LF2). F) Logged section through laterally continuous series
1167 of amalgamated sandstones (LF1). G) Logged sections of laterally discontinuous thin-bedded
1168 turbidites (LF3), laterally continuous thin-bedded turbidites (LF4), a rare hybrid event bed
1169 (LF5) and bioclastic grit (LF6). Log locations shown on log 1 in Figure 5.

1170

1171 Fig. 5. Logged sections L1 and L2 through the thick-bedded, amalgamated sandstones in the
1172 Owahanga Gorge (Fig. 3). Petrophysical data displayed for L2. Logged section L3 from the

heterolithic overlying section. Inset map showing extent of lithofacies association 1 (LA1) in the Owahanga Gorge area, with the location of the three illustrated logs. Detailed logs and full petrophysical data are available in supplementary material; key to symbols in Figure 4. LC = lobe complex.

Fig. 6. A) Photo panel of lobe fringe (LA2) section in Pongaroa Stream. B) Interpretation of the outcrop, which is mostly composed of laterally continuous thin-beds (LF4), but with minor laterally continuous (LF1) and laterally discontinuous thick-bedded sandstones (LF2). C) Photo panel of the top of log L3, showing thin- to thick-bedded turbidites of LA2 truncated and overlain by chaotic siltstones of LA3.

Fig. 7. Logged sections L4, L5, L6 and L7 through the Upper Burdigalian heterolithics on the western side of the Akitio Basin, LA2 as beige coloured map unit (Fig. 3). Note occurrences of thick mudstone intervals, e.g. at 47 m, 53 m and 57 m up log L7 and 32 m, 83 m and 116 m up log L4. Mapped extent of lithofacies association 2 (LA2) in the western limb of the Akitio Syncline, showing location of the illustrated logs. Detailed logs and petrophysical data are available in supplementary material.

Fig. 8. Quantitative observations including a breakdown of sediment type, style of structures, palaeocurrents and bed thickness from A) Lithofacies association 1, dominated by tabular, thick-bedded, sandstones (LF1) intercalated with irregular thin-beds (LF3), lenticular, thick-bedded, sandstones (LF2) and rarely hybrid event beds (HEB; LF5). Amalgamated beds up to 2 m thick traceable over 100's of m, in a unit 200 m thick and >5 km wide. Average net to

gross 86%; foraminifera water depth mid bathyal (>700 m). Deposition from dominantly high to low-density, high-concentration turbidity currents, with bypass of finer suspension cloud particles due to flow stripping. B) Lithofacies association 2, laterally continuous thin-beds (LF4) with sporadic tabular thick-beds (LF1), separated by mudstones (LF7), hybrid event beds (LF5) and rare lenticular, thick-bedded, sandstones (LF2) in packages tens to hundreds of metres thick occurring across the sub-basin where LA1 not present. Average net to gross 40%; foraminifera water depth mid bathyal (>700 m). Deposition from dominantly waning, low-density turbidity currents, periodically with influxes of higher concentration turbidity currents and flow transformations resulting in hybrid event debris flows.

Fig. 9. Petrophysical logs and correlation of logged sections L2 and L5, illusrating the development and correlation of seven lobe complexes. Age abbreviations as Fig. 2. LC = lobe complex.

Fig. 10. Top: Non-interpreted dip profile seismic cross-section of the Porangahau Trough and Ridge (see location in Fig 1, respectively PT and PR). Bottom: Interpreted section highlighting the evolution of the basin fill and structures. Seismic facies 1 represents the background, non-shaded intervals. SA = Seismic facies associations. Note 2x vertical exaggeration.

Fig. 11. (A) Detailed seismic dip line across the Porangahau Trough (PT) and Porangahau Ridge (PR). (B) Interpretation of dip line. (C) Strike line along the Porangahau Trough. (D) Interpretation of strike line. (E) Dip line from (A) flattened on base lobes (SF4). (F)

Interpretation of flattened lobes and MTDs (SA2). (G) Dip and strike lines, and depth slice of basal lobe complex. (H) Interpretation of G (SA2). Note dip and strike lines intersect in the middle of the view. Seismic facies 1 represents the background, non-shaded intervals. SA = Seismic facies associations. Note 4x vertical exaggeration in A-F.

Fig. 12. A) Root-mean-square (RMS) amplitude horizon along the studied subsurface Madden channel – lobe system, highlighting the otherwise low amplitude response across the margin during the study interval. The detailed area, linked cross-sections of the Porangahau Trough (PT), Ridge (PR) and the next downstream basin, and step by step horizons is shown in B-G, which represent ca. 50 m intervals through the lobe system, a systematic view through all reflectors is provided in the supplementary video. B) Below the lobe complexes, with feeder channel supplying sediment into a fully ponded and silled basin. C) First lobe complex developing at mouth of feeder channel; note subsequent erosion within the channel, likely related to later MTD emplacement excising an up-dip portion of the lobes. D) Second lobe complex, displaying distributary channels. E) Third lobe complex; up until this point the bypassing fines are inferred to be below seismic resolution but from here on a gradual brightening of the downstream basin is seen. F) Upper lobe complex, displaying lower RMS response and potential spill of fine-grained material into the downstream basin and erosion of the sill crest. G) Termination of the lobe system by emplacement of a low amplitude (muddy) mass-transport deposit (MTD). Maps are displayed so as low amplitude reflectors (i.e., fine-grained deposits) are in dull black to grey colours whilst the high amplitude (i.e., coarser grained deposits) are displayed in bright colours.

Fig. 13. Cross-plot of lobe system thicknesses and lengths from a range of deep-water lobes across the globe. Other than results from this study, data was extracted from Flood et al. (1991); Horine et al. (2000); Pirmez et al. (2000); Piper and Normark (2001); Popescu et al. (2001); Grecula et al. (2003); Sixsmith et al. (2004); Van Lente (2004); Deptuck et al. (2008); Jegou et al. (2008); Iorio et al. (2009); Bourget et al. (2010); Figueiredo et al. (2010, 2013); Pringle et al. (2010); Flint et al. (2011); Brunt et al. (2013); Lericolais et al. (2013); Burgreen and Graham (2014); Yang and Kim (2014): Hofstra et al. (2015): Tinterri and Tagliaferri (2015); Zhang et al. (2016); Dennielou et al. (2017); Jobe et al. (2017, 2018); Liu et al. (2018); Postma and Kleverlaan (2018); Pyles et al. (2019); Tinterri and Piazza (2019).

Fig. 14. Schematic flow process and kinematic model for sediment – structure interaction from time 0 – 4. Initially sediments entering the basin pond within the centre, onlap edges and intra-basinal structures (T0). Subsequent sediment influx supresses intra-basinal structures, focusing stress on basin-bounding structures (T1-3). If the growth of Thrust 1 [F1] and Thrust 2 [F2] are similar and the net sediment flux [S] balances the rate at which accommodation space is generated (by tectonic [T] and isostatic loading [L]) then aggradationally-stacked lobe complexes (LC) may develop. Under this scenario dynamic growth of basin-bounding structures maintain sills and perpetuate flow stripping, trapping coarse material behind the down-slope sill, whilst allowing downstream bypass of fines. This equilibrium is eventually disrupted by allogenic factors, here being emplacement of a regional mass-transport deposit.

Fig. 15. Schematic tectono-stratigraphic evolution model of trench-slope basin fill. A-C show allogenic control by flow stripping at the downstream sill, resulting in trapping of coarse-

grained lobe systems behind the sill with bypass of fine-grained particles downstream. D) Ultimately, an autogenic influence (here emplacement of a mass-transport deposit) results in fundamental modification of the sedimentary system, basin dynamics and disrupting the balance between sedimentation and deformation.

Fig. 16. Schematic Gamma Ray (GR) wireline log motifs and composite (Comp) logs for a lobe complex fringe, axis, bypass edge and downstream basin. Note bypass thin beds are not laterally extensive and may not present a barrier to fluid flow, unlike the blanketing fines of the fringe or downstream basin.

## SUPPLEMENTARY MATERIAL CAPTIONS

A. Detailed sedimentary logs 1-7. Log 1 location start 176.2732, -40.6301; finish 176.2741, -40.6254. Log 2 start 176.2774, -40.6275; finish 176.2758, -40.6250. Log 3 coordinates start 176.2727, -40.6214; finish 176.2744, -40.6206. Log 4 start 176.2194, -40.5547; finish 176.2236, -40.5611. Log 5 176.2162, -40.5565. Log 6 176.2221, -40.5638. Log 7 start 176.2212, -40.5557; finish 176.2260, -40.5588.

B. Gamma Ray and clay minerals data from logged sections L2 and L5.

C. Video of all mapped horizons, from the subsurface example. Video covers from emplacement of lower MTD, through the higher amplitude lobe complexes to the termination of the lobe system by emplacement and incision by the upper MTD.

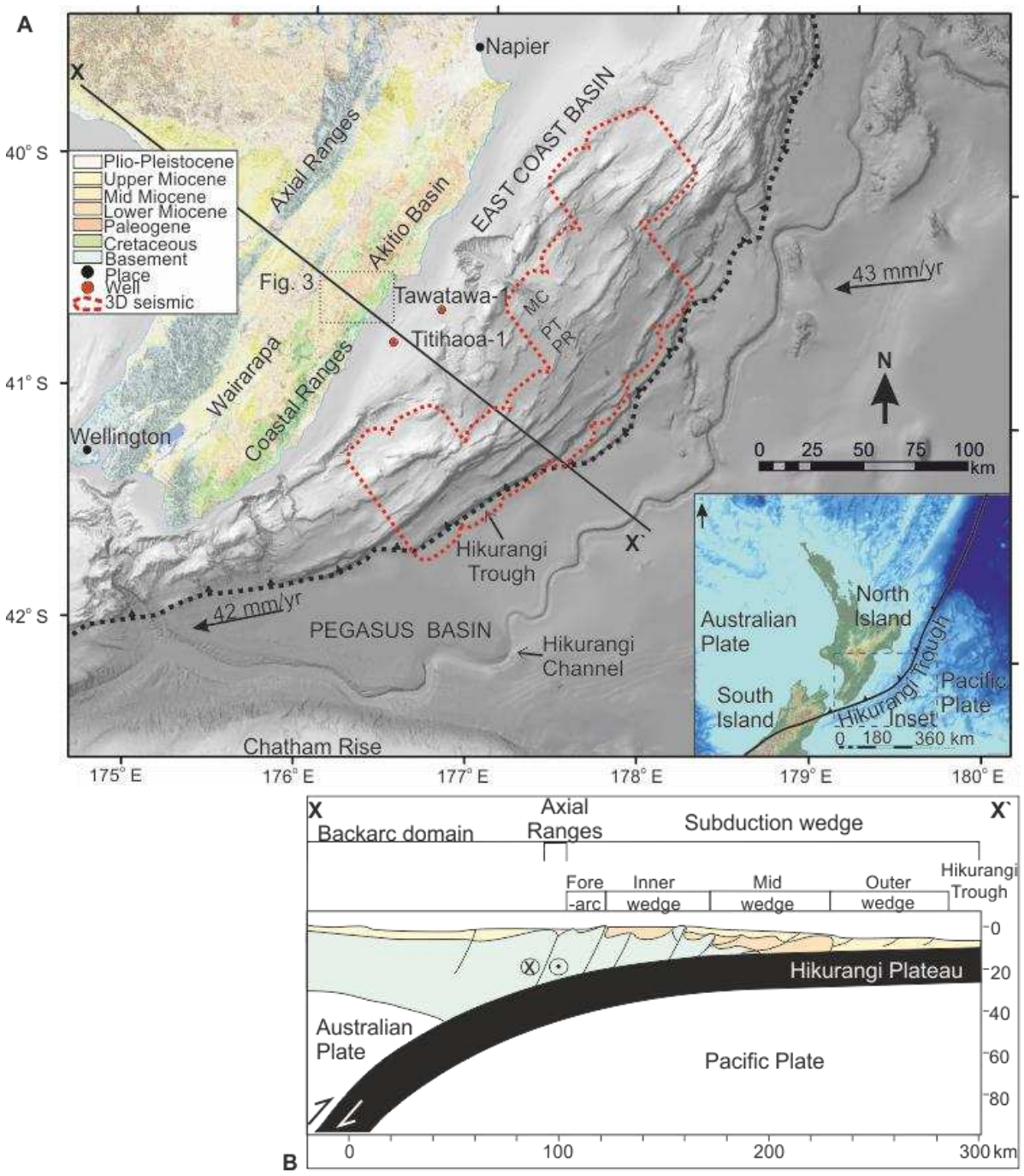
A
X
X`
Napier
Plio-Pleistocene
Upper Miocene
Mid Miocene
Lower Miocene
Paleogene
Cretaceous
Basement
Place
Well
3D seismic
Axial Ranges
Akitio Basin
EAST COAST BASIN
Fig. 3
Tawatawa-1
Titihaoa-1
MC
PT
PR
43 mm/yr
N
0 25 50 75 100 km
Wairarapa
Coastal Ranges
Wellington
Hikurangi Trough
42 mm/yr
PEGASUS BASIN
Hikurangi Channel
Chatham Rise
40° S
41° S
42° S
175° E
176° E
177° E
178° E
179° E
180° E
Australian Plate
North Island
South Island
Pacific Plate
Hikurangi Trough
Inset
0 180 360 km
B
X
X`
Backarc domain
Axial Ranges
Subduction wedge
Fore -arc
Inner wedge
Mid wedge
Outer wedge
Hikurangi Trough
Hikurangi Plateau
Australian Plate
Pacific Plate
0
20
40
60
80
0
100
200
300 km

1288

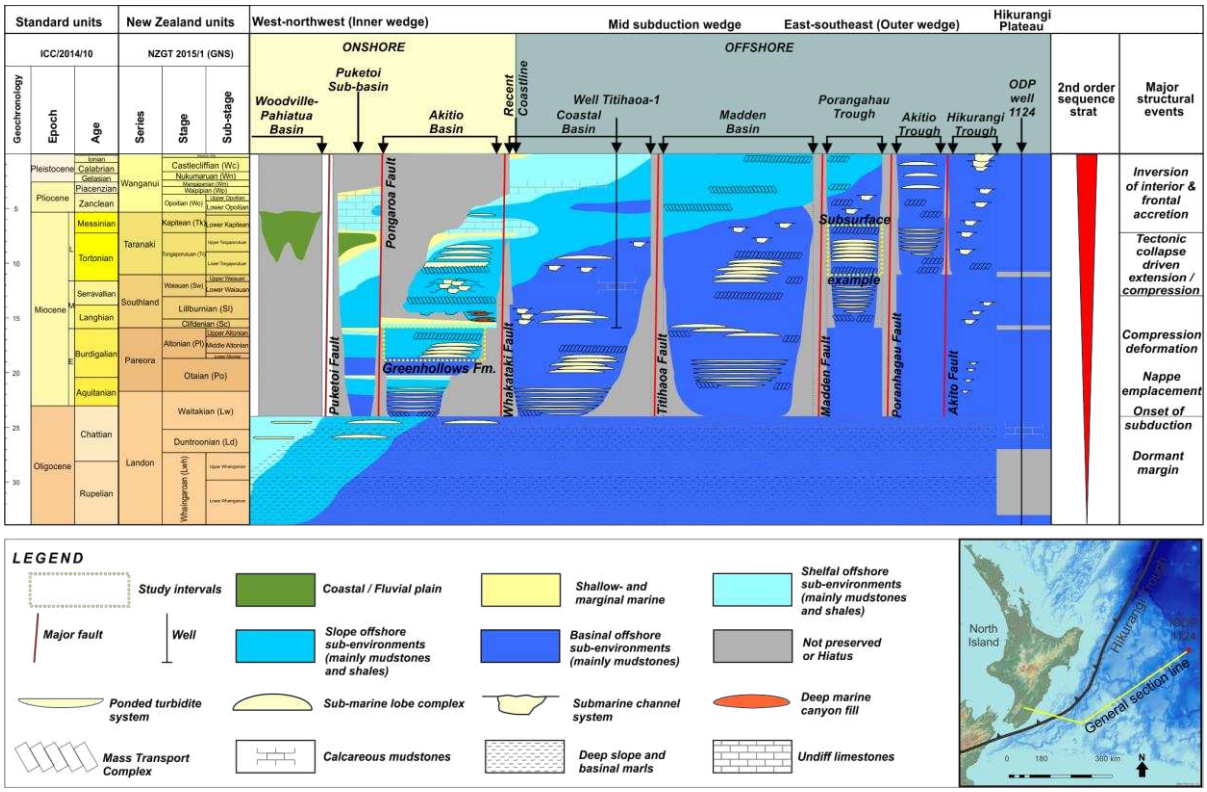


1289

1290

1291

1292

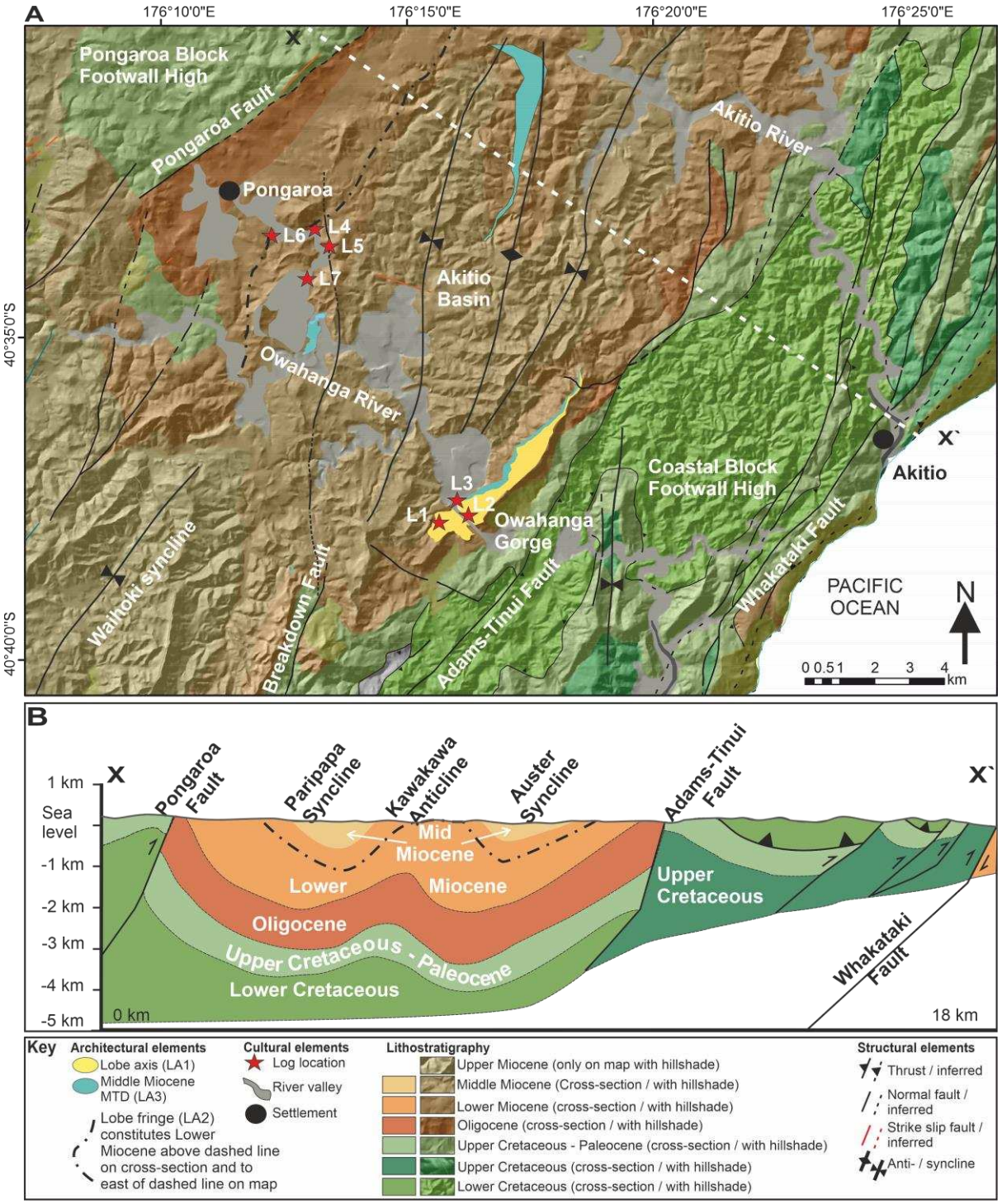
A
176°10'0"E
176°15'0"E
176°20'0"E
176°25'0"E
40°35'0"S
40°40'0"S
Pongaroa Block Footwall High
Pongaroa Fault
Pongaroa
L6
L4
L5
L7
Akitio Basin
Akitio River
Owahanga River
L3
L2
L1
Owahanga Gorge
Coastal Block Footwall High
Akitio
Waihoki syncline
Breakdown Fault
Adams-Tinui Fault
Whakataki Fault
PACIFIC OCEAN
N
0 0.5 1 2 3 4 km
B
1 km
Sea level
-1 km
-2 km
-3 km
-4 km
-5 km
Pongaroa Fault
Paripapa Syncline
Kawakawa Anticline
Auster Syncline
Adams-Tinui Fault
Mid Miocene
Lower Miocene
Oligocene
Upper Cretaceous - Paleocene
Lower Cretaceous
Upper Cretaceous
Whakataki Fault
0 km
18 km
Key
Architectural elements
Lobe axis (LA1)
Middle Miocene MTD (LA3)
Lobe fringe (LA2) constitutes Lower Miocene above dashed line on cross-section and to east of dashed line on map
Cultural elements
Log location
River valley
Settlement
Lithostratigraphy
Upper Miocene (only on map with hillshade)
Middle Miocene (Cross-section / with hillshade)
Lower Miocene (cross-section / with hillshade)
Oligocene (cross-section / with hillshade)
Upper Cretaceous - Paleocene (cross-section / with hillshade)
Upper Cretaceous (cross-section / with hillshade)
Lower Cretaceous (cross-section / with hillshade)
Structural elements
Thrust / inferred
Normal fault / inferred
Strike slip fault / inferred
Anti- / syncline

1293

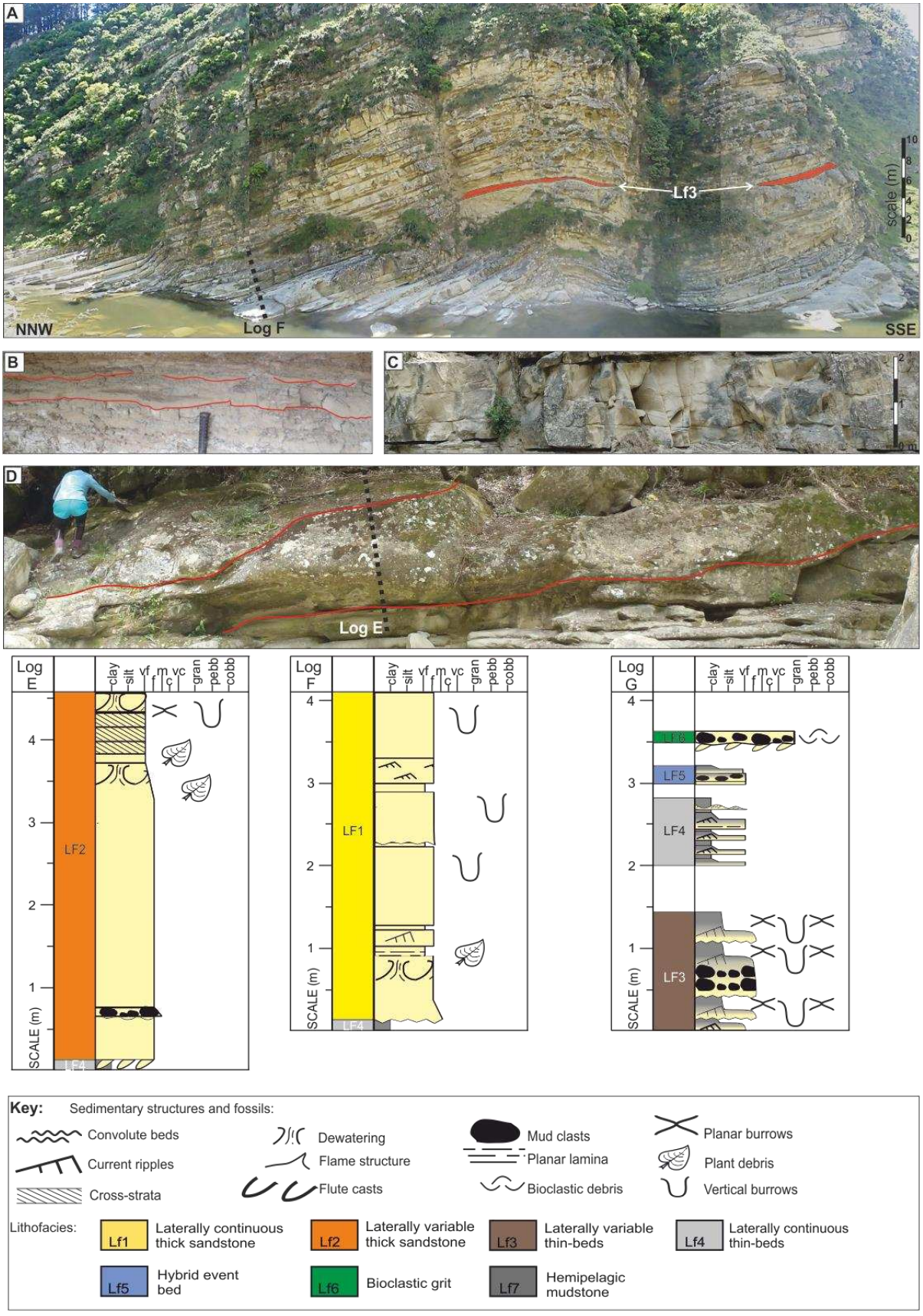
A
Lf3
scale (m)
NNW
Log F
SSE
B
C
D
Log E
Log E
clay silt vf f m c vc gran pebb cobb
LF2
LF1
SCALE (m)
Log F
Log G
LF6
LF5
LF4
LF3
Key: Sedimentary structures and fossils:
Convolute beds
Current ripples
Cross-strata
Dewatering
Flame structure
Flute casts
Mud clasts
Planar lamina
Bioclastic debris
Planar burrows
Plant debris
Vertical burrows
Lithofacies:
Lf1 Laterally continuous thick sandstone
Lf2 Laterally variable thick sandstone
Lf3 Laterally variable thin-beds
Lf4 Laterally continuous thin-beds
Lf5 Hybrid event bed
Lf6 Bioclastic grit
Lf7 Hemipelagic mudstone

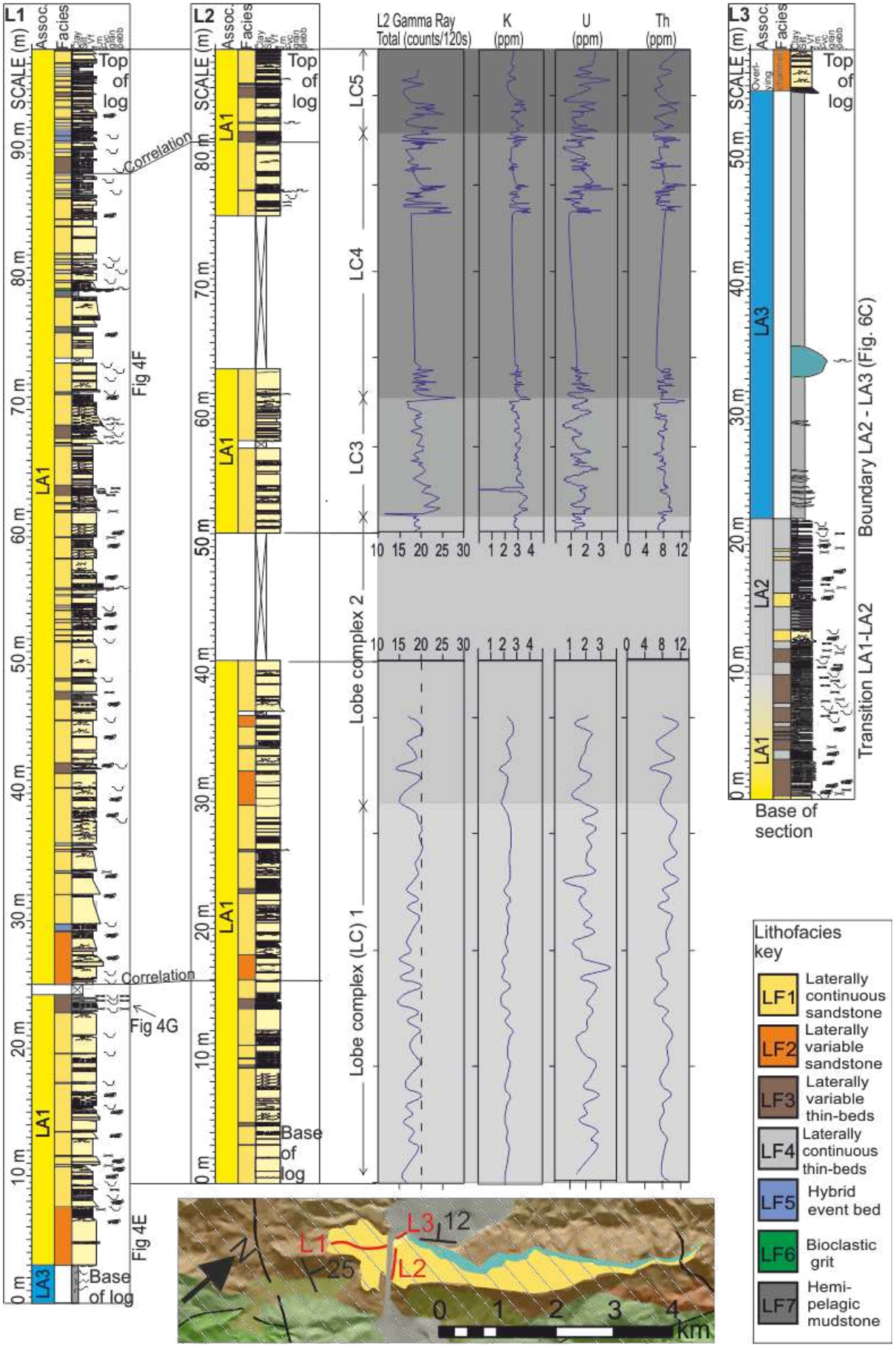
L1
L2
L3
Assoc.
Facies
SCALE (m)
Top of log
Base of log
Correlation
Fig 4F
Fig 4G
Fig 4E
LA1
LA2
LA3
L2 Gamma Ray Total (counts/120s)
K (ppm)
U (ppm)
Th (ppm)
LC5
LC4
LC3
Lobe complex 2
Lobe complex (LC) 1
Boundary LA2 - LA3 (Fig. 6C)
Transition LA1-LA2
Base of section
L1
L2
L3
12
25
0 1 2 3 4 km
Lithofacies key
LF1 Laterally continuous sandstone
LF2 Laterally variable sandstone
LF3 Laterally variable thin-beds
LF4 Laterally continuous thin-beds
LF5 Hybrid event bed
LF6 Bioclastic grit
LF7 Hemi-pelagic mudstone

1297

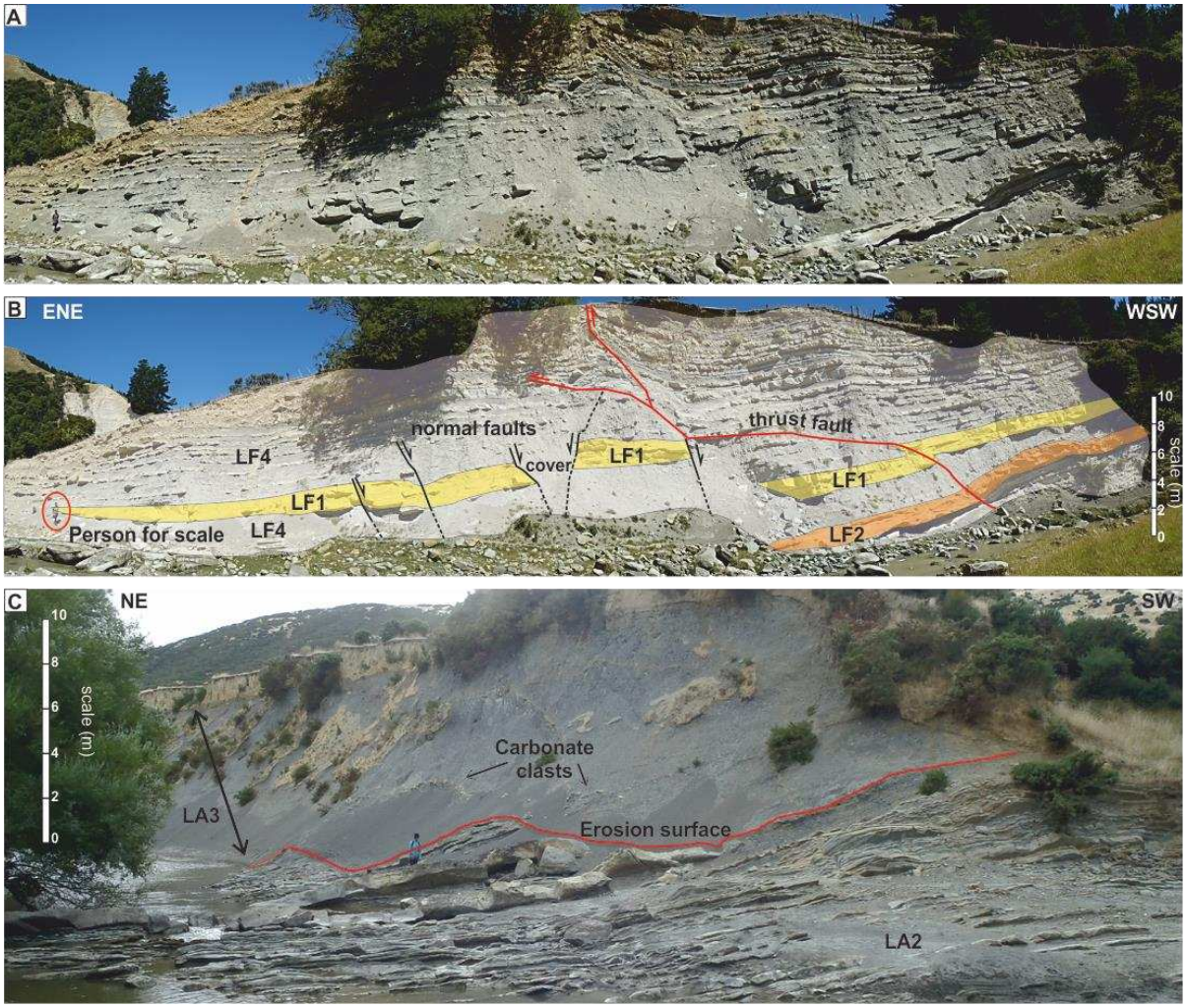


1298

1299

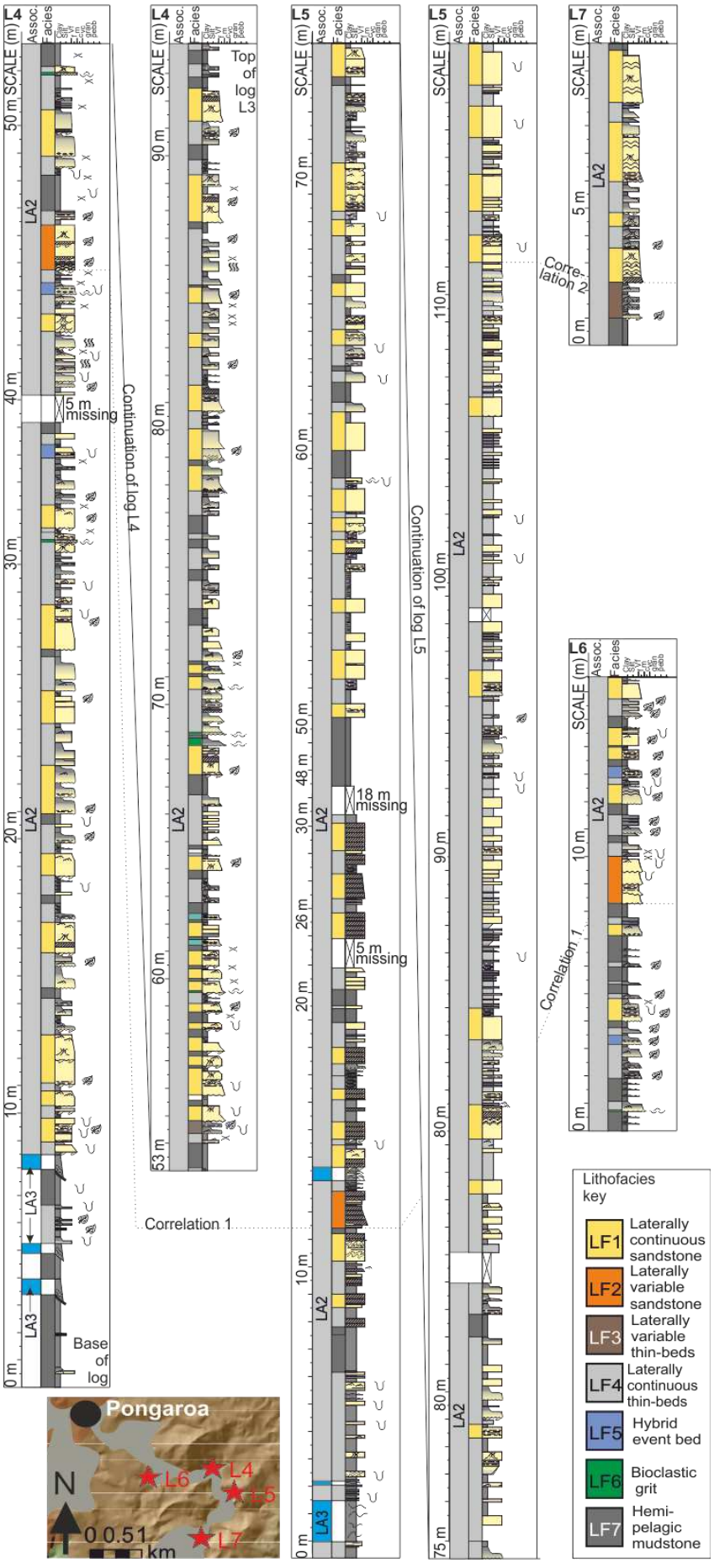
L4
L4
L5
L5
L7
L6
SCALE (m)
Assoc.
Facies
LA2
LA3
Top of log L3
5 m missing
18 m missing
Base of log
Continuation of log L4
Continuation of log L5
Correlation 1
Correlation 2
Pongaroa
N
0 0.5 1 km
L4
L5
L6
L7
Lithofacies key
LF1 Laterally continuous sandstone
LF2 Laterally variable sandstone
LF3 Laterally variable thin-beds
LF4 Laterally continuous thin-beds
LF5 Hybrid event bed
LF6 Bioclastic grit
LF7 Hemi-pelagic mudstone

**A) Lithofacies association 1 - lobe axis**

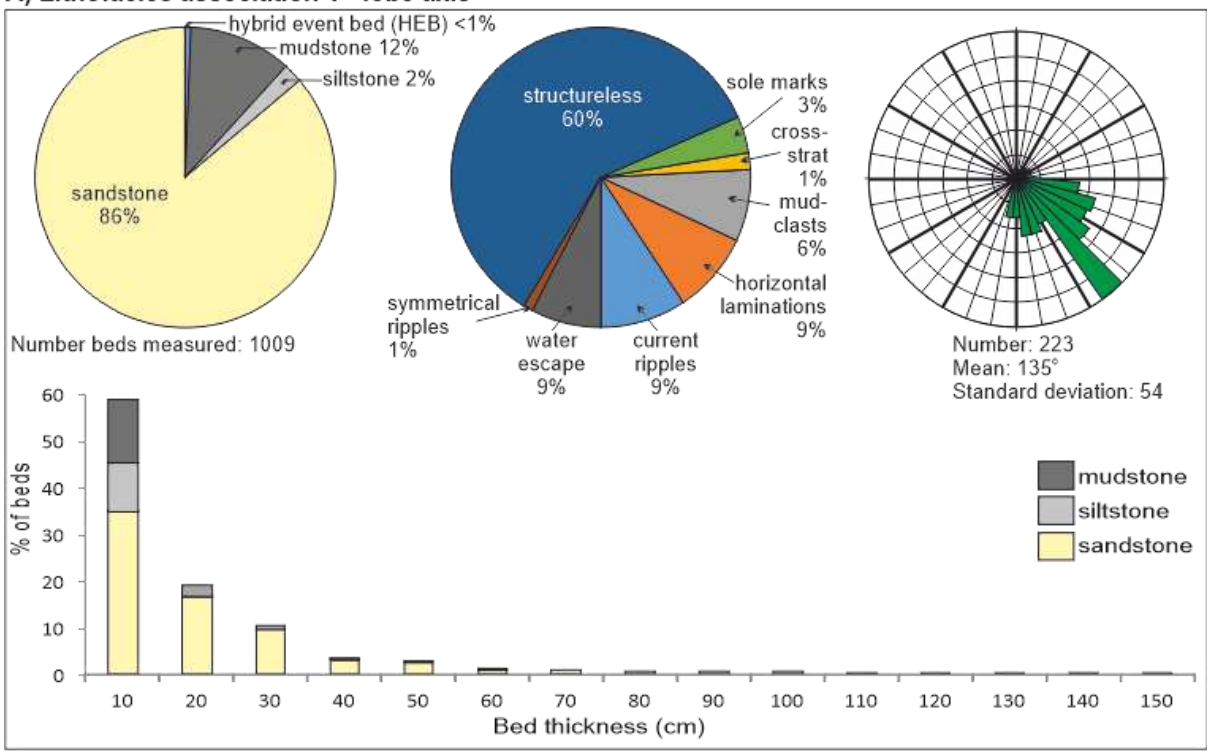


**Lithofacies association 2 - lobe fringe**

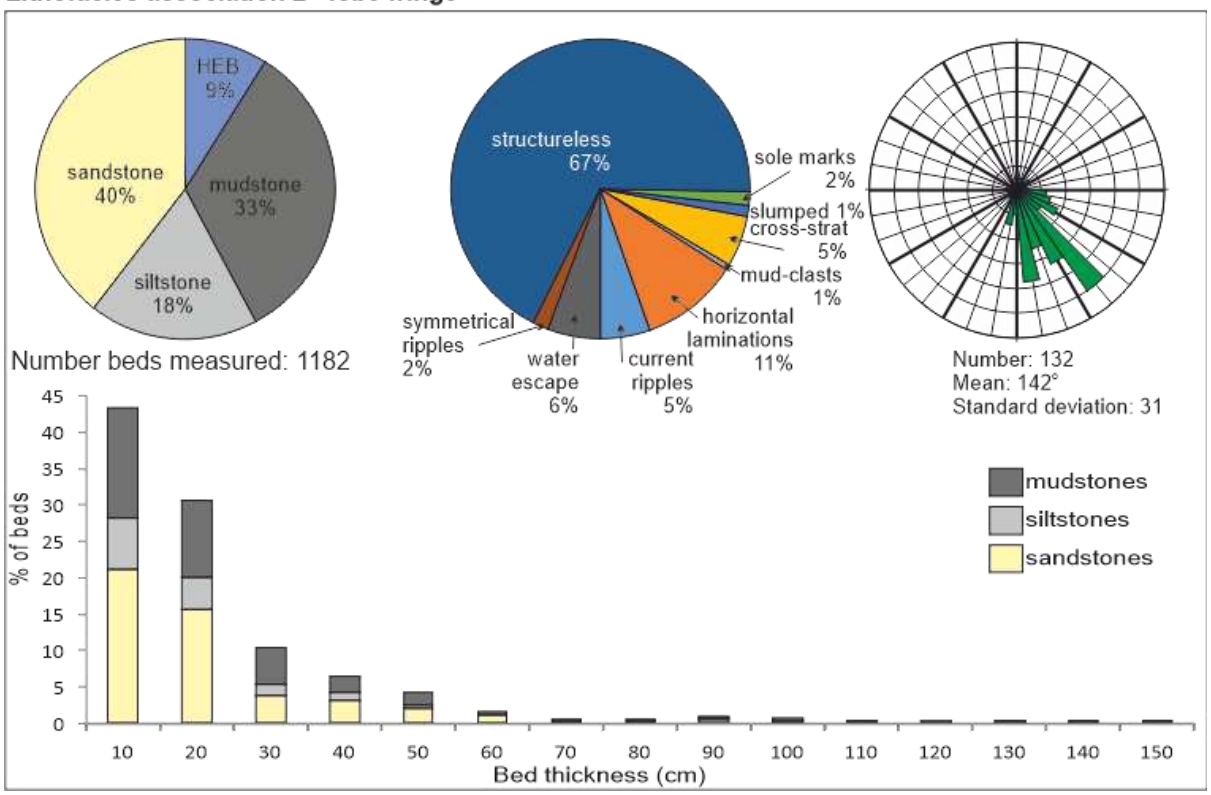

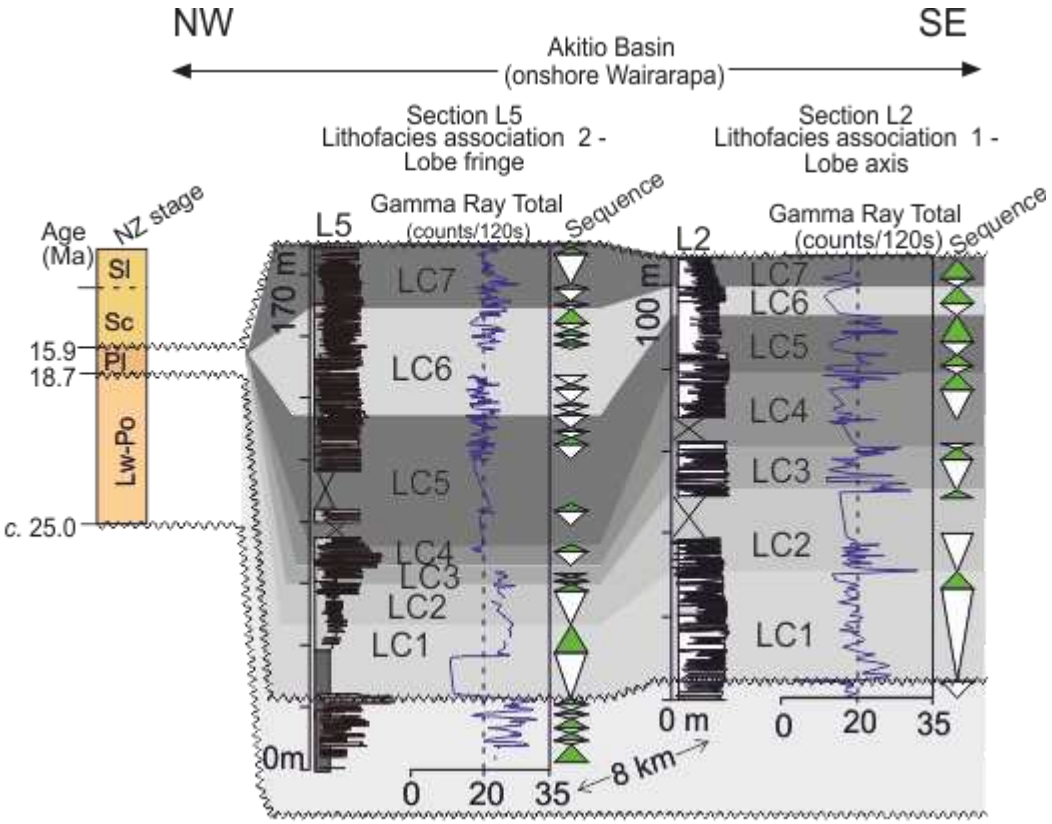
NW
SE
Akitio Basin
(onshore Wairarapa)
Section L5
Lithofacies association 2 -
Lobe fringe
Section L2
Lithofacies association 1 -
Lobe axis
Age
(Ma)
NZ stage
Sl
Sc
Pl
Lw-Po
15.9
18.7
c. 25.0
L5
Gamma Ray Total
(counts/120s)
Sequence
170 m
0m
LC7
LC6
LC5
LC4
LC3
LC2
LC1
0
20
35
8 km
L2
Gamma Ray Total
(counts/120s)
Sequence
100 m
0 m
LC7
LC6
LC5
LC4
LC3
LC2
LC1
0
20
35

1303

1304

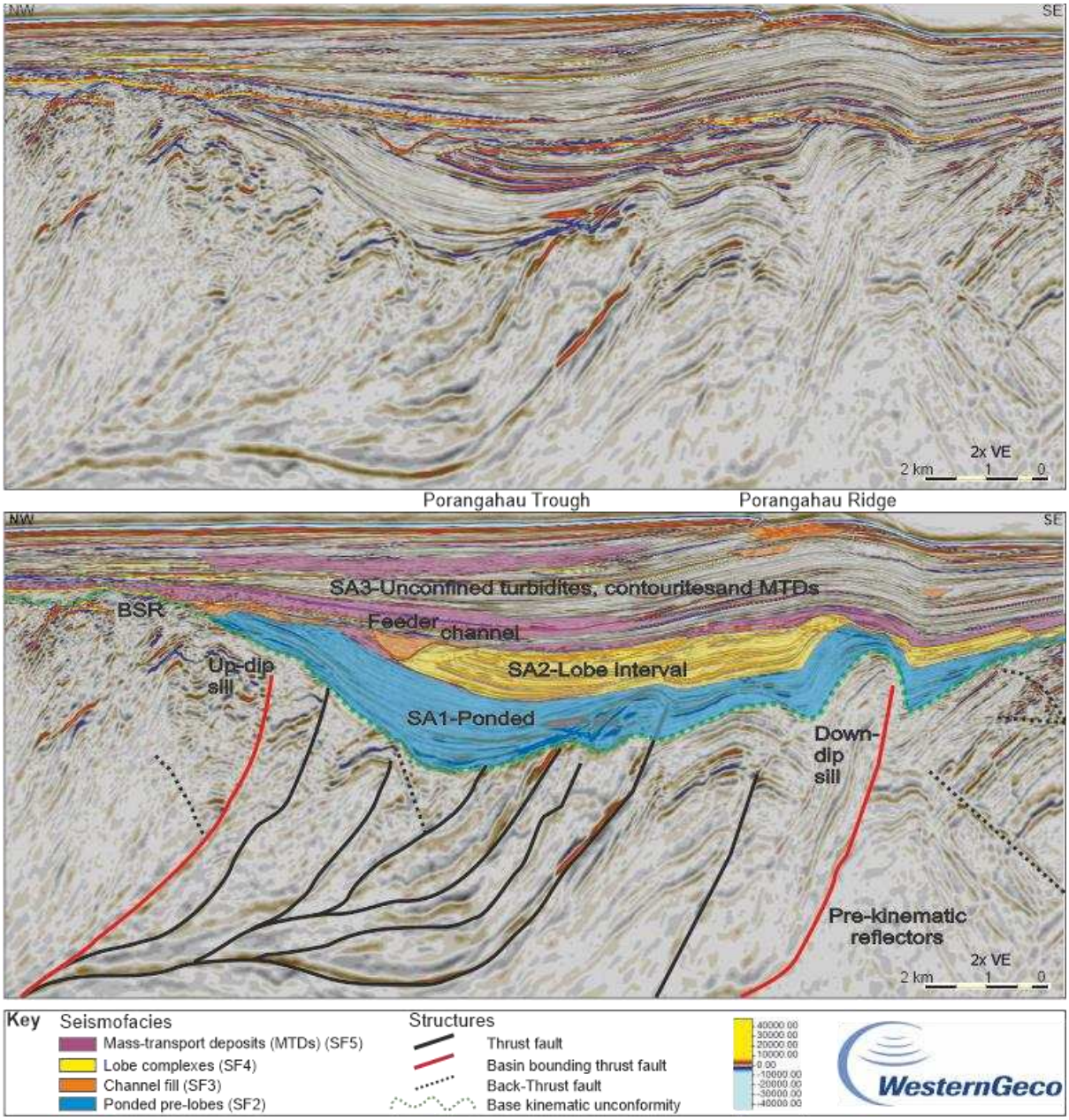
NW
SE
2 km
2x VE
1
0
Porangahau Trough
Porangahau Ridge
NW
SE
SA3-Unconfined turbidites, contouritesand MTDs
BSR
Feeder channel
Up-dip sill
SA2-Lobe Interval
SA1-Ponded
Down-dip sill
Pre-kinematic reflectors
2 km
2x VE
1
0
Key
Seismofacies
Mass-transport deposits (MTDs) (SF5)
Lobe complexes (SF4)
Channel fill (SF3)
Ponded pre-lobes (SF2)
Structures
Thrust fault
Basin bounding thrust fault
Back-Thrust fault
Base kinematic unconformity
WesternGeco

1305

1306

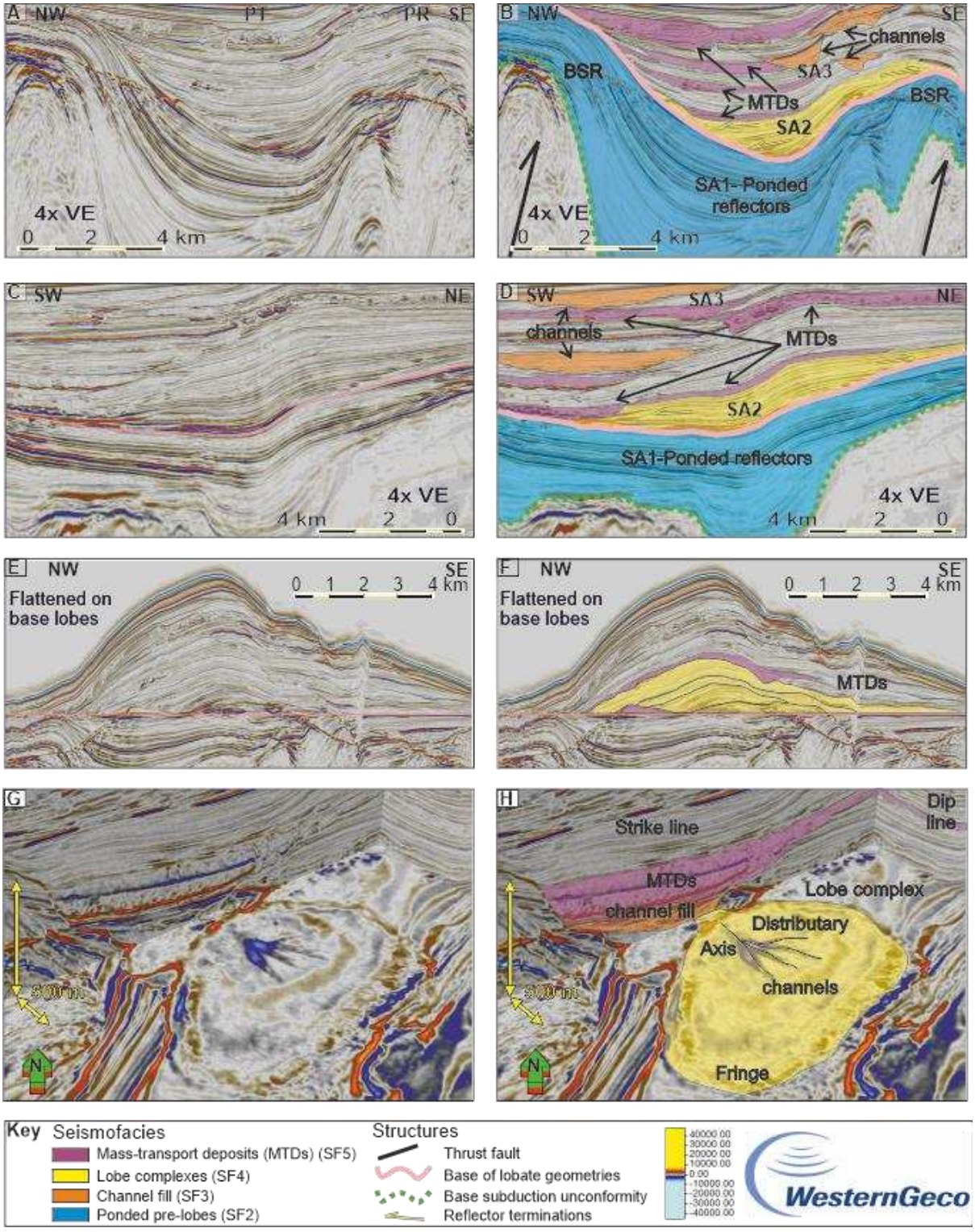
A NW
PT
PR SE
4x VE
0 2 4 km
B NW
SE
channels
BSR
SA3
MTDs
BSR
SA2
SA1-Ponded reflectors
4x VE
0 2 4 km
C SW
NE
4x VE
4 km 2 0
D SW
SA3
NE
channels
MTDs
SA2
SA1-Ponded reflectors
4x VE
4 km 2 0
E NW
SE
0 1 2 3 4 km
Flattened on base lobes
F NW
SE
0 1 2 3 4 km
Flattened on base lobes
MTDs
G
5,000 ms
N
H
Strike line
Dip line
MTDs
channel fill
Lobe complex
Distributary
Axis
channels
Fringe
5,000 ms
N
Key
Seismofacies
Mass-transport deposits (MTDs) (SF5)
Lobe complexes (SF4)
Channel fill (SF3)
Ponded pre-lobes (SF2)
Structures
Thrust fault
Base of lobate geometries
Base subduction unconformity
Reflector terminations
WesternGeco

1307

1308

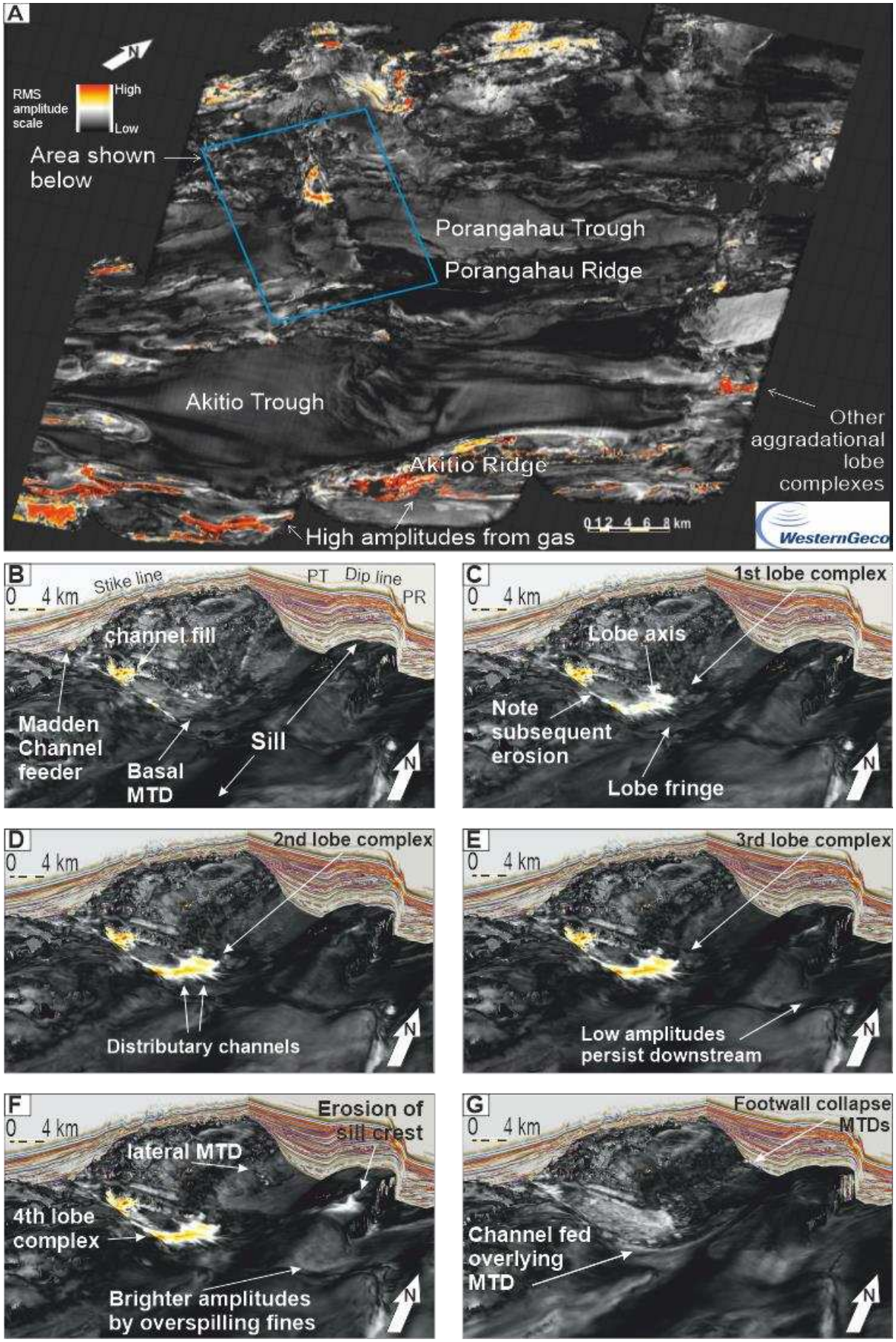
A
N
RMS amplitude scale
High
Low
Area shown below
Porangahau Trough
Porangahau Ridge
Akitio Trough
Akitio Ridge
Other aggradational lobe complexes
High amplitudes from gas
0 1 2 4 6 8 km
WesternGeco
B
0 4 km
Stike line
PT
Dip line
PR
channel fill
Madden Channel feeder
Basal MTD
Sill
N
C
0 4 km
1st lobe complex
Lobe axis
Note subsequent erosion
Lobe fringe
N
D
0 4 km
2nd lobe complex
Distributary channels
N
E
0 4 km
3rd lobe complex
Low amplitudes persist downstream
N
F
0 4 km
Erosion of sill crest
lateral MTD
4th lobe complex
Brighter amplitudes by overspilling fines
N
G
0 4 km
Footwall collapse MTDs
Channel fed overlying MTD
N

1309

1310

1311

1312

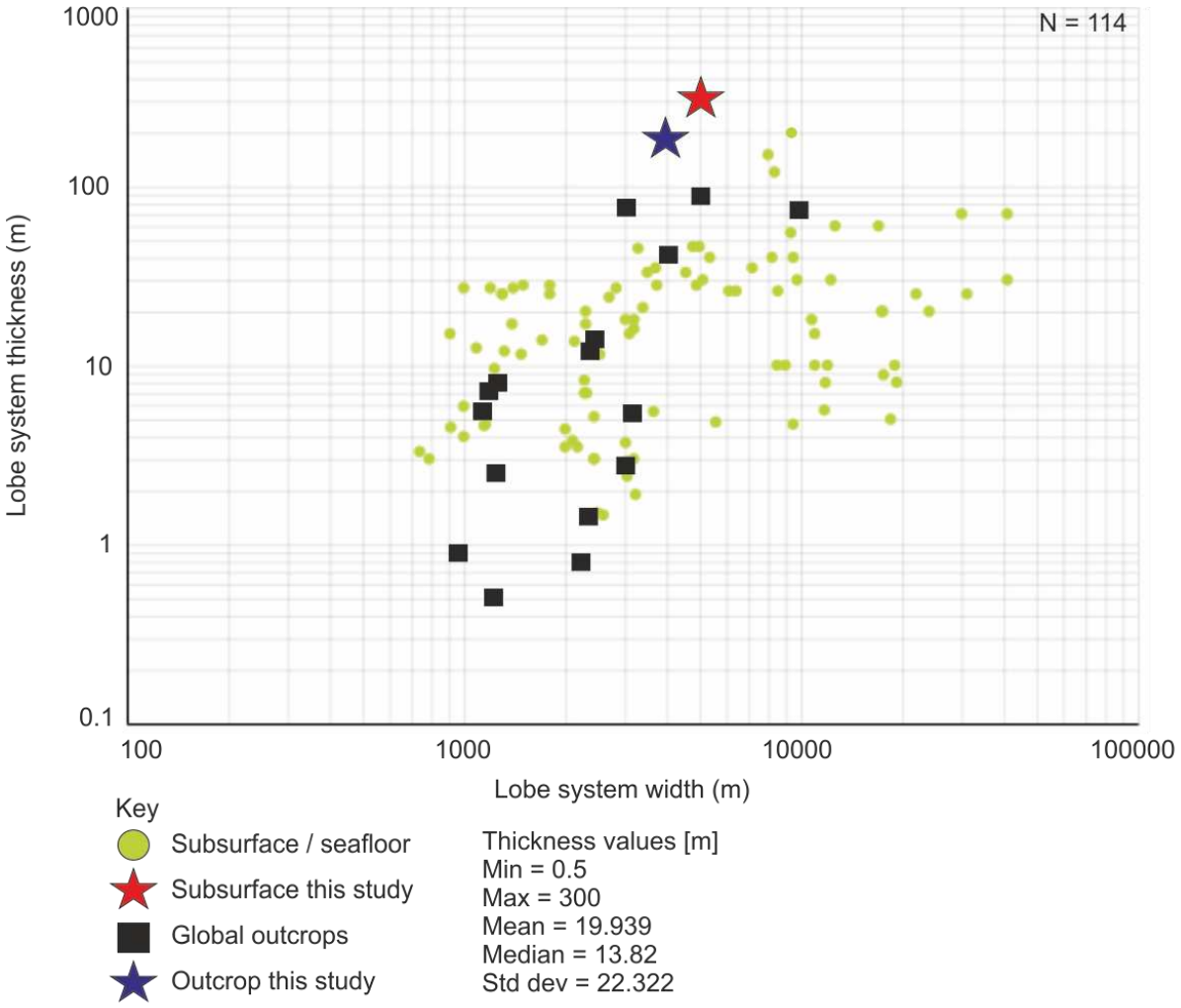


1313

1314

1315

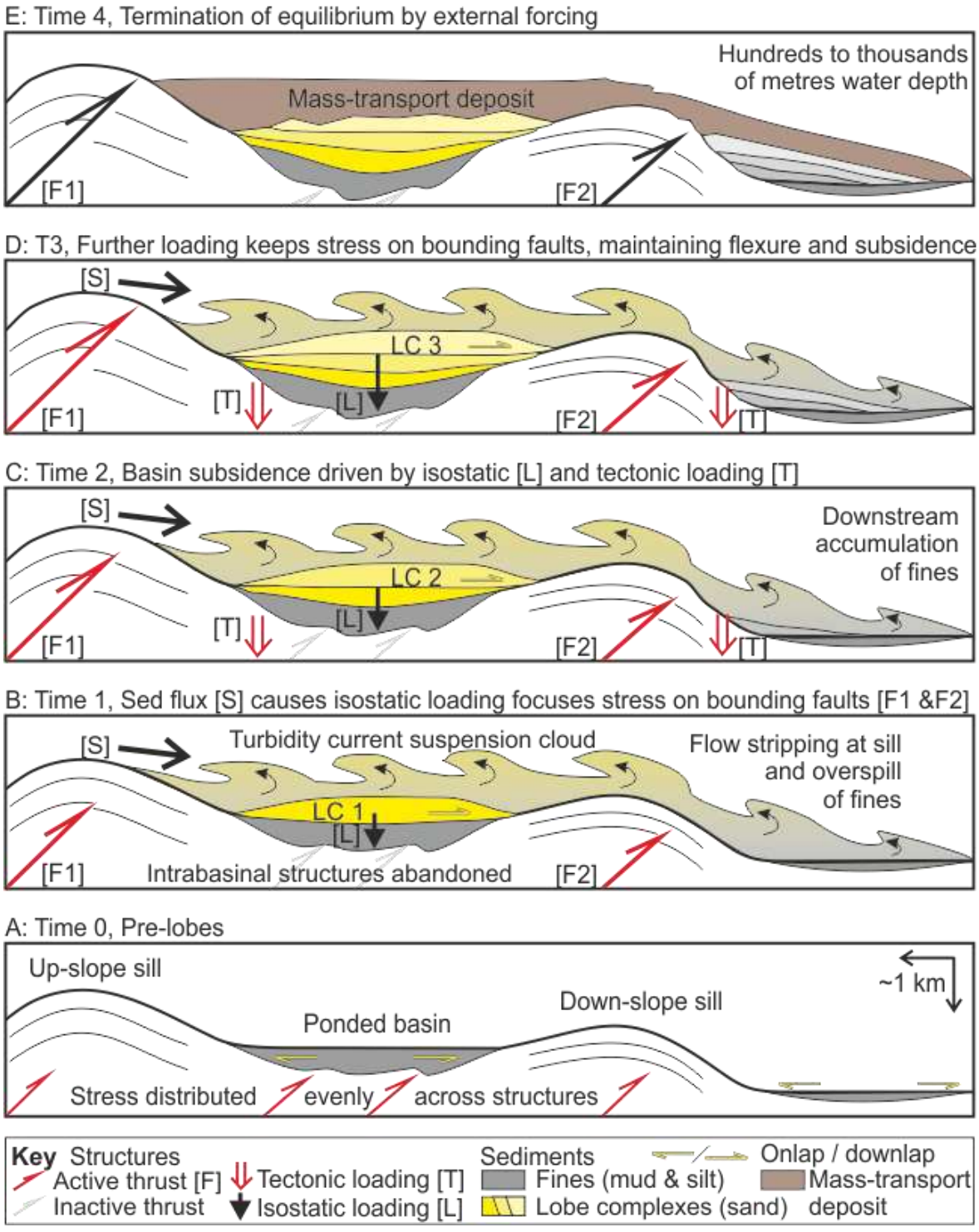


1316

1317

1318

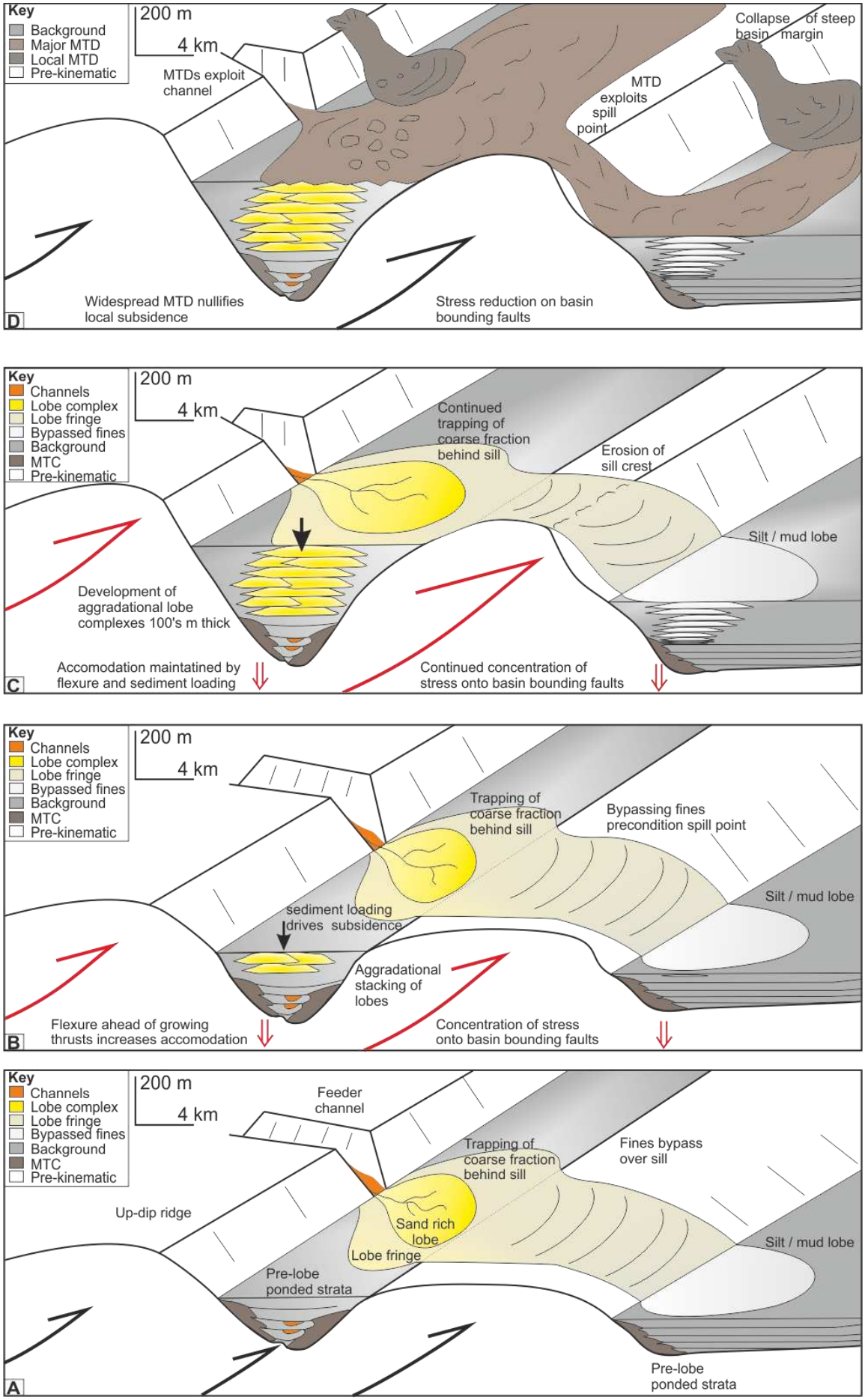
Key
Background
Major MTD
Local MTD
Pre-kinematic
200 m
4 km
MTDs exploit channel
Collapse of steep basin margin
MTD exploits spill point
Widespread MTD nullifies local subsidence
Stress reduction on basin bounding faults
D
Key
Channels
Lobe complex
Lobe fringe
Bypassed fines
Background
MTC
Pre-kinematic
200 m
4 km
Continued trapping of coarse fraction behind sill
Erosion of sill crest
Silt / mud lobe
Development of aggradational lobe complexes 100's m thick
Accomodation maintatined by flexure and sediment loading
Continued concentration of stress onto basin bounding faults
C
Key
Channels
Lobe complex
Lobe fringe
Bypassed fines
Background
MTC
Pre-kinematic
200 m
4 km
Trapping of coarse fraction behind sill
Bypassing fines precondition spill point
Silt / mud lobe
sediment loading drives subsidence
Aggradational stacking of lobes
Flexure ahead of growing thrusts increases accomodation
Concentration of stress onto basin bounding faults
B
Key
Channels
Lobe complex
Lobe fringe
Bypassed fines
Background
MTC
Pre-kinematic
200 m
4 km
Feeder channel
Trapping of coarse fraction behind sill
Fines bypass over sill
Up-dip ridge
Sand rich lobe
Lobe fringe
Silt / mud lobe
Pre-lobe ponded strata
Pre-lobe ponded strata
A

1319

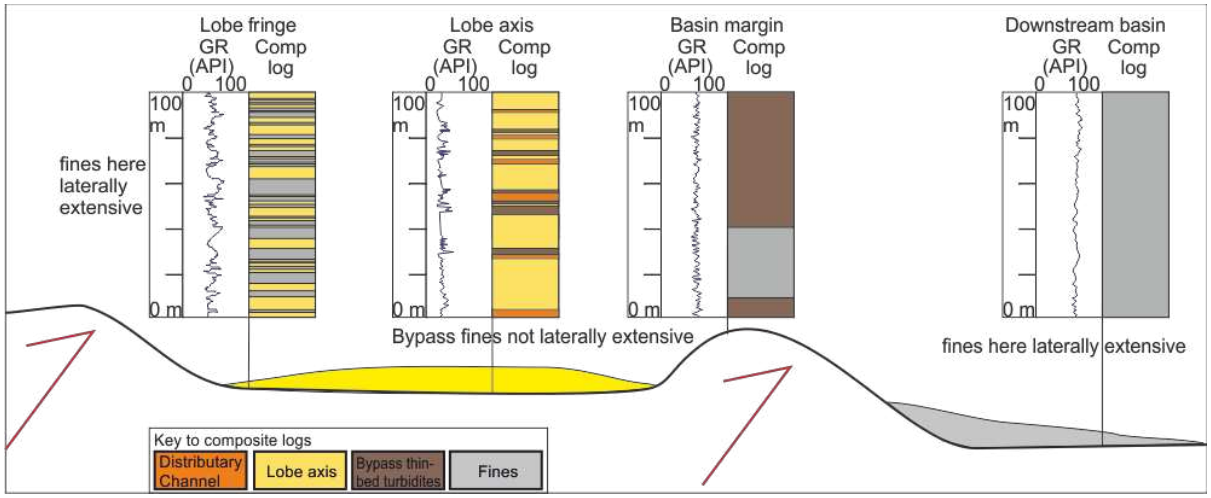


1320

1321

1322

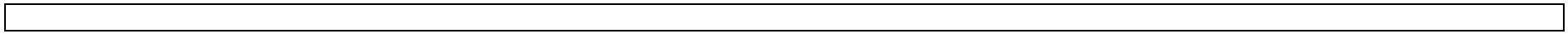

1323

Table 1. Principal lithofacies types of the Greenhollows Formation examined in the present study.

| | | |
|---|---|---|
| | Lithofacies 1: Tabular, medium to thick-bedded sandstone<br>Description: Pale grey to beige, graded beds up to 2m thick of fine to very fine-grained, well-sorted sandstone. Bed bases are typically irregular and may truncate underlying strata by up to 10 cm; sole marks, primarily flutes are common. The bases may initially show inverse grain size grading. The lowermost portion (lower 5-10 cm) of beds may show planar lamination, often highlighted by carbonaceous bands, but planar cross-stratification was also observed. Above this the beds are typically massive and or dewatered. The upper portion may show a return to planar and ripple lamination. This is an idealised succession and beds may show a different order or not all of the structures. Variably sole marks, cross-strata and ripples may show subtly different orientations (Fig. 8). Sandstones are often amalgamated; rare trains of internal mud-clasts or grain size breaks may mark amalgamation surfaces. Mud-clasts may also occur scattered throughout individual beds. These beds are tabular and may be traced over tens to hundreds of meters across any one outcrop. | Interpretation: These sandstones are interpreted as the deposition from high to low-density, high-concentration turbidity currents (sensu Lowe, 1982), with current re-working. Massive portions were likely deposited under upper stage flow regimes, with high sediment fallout rates, but could also have lost structures due to dewatering; both processes indicating rapid deposition. Cross-strata, the thickness of beds and climbing ripples imply sustained flows. Waning flows may have resulted in the gradational upper portion of beds (Bouma Ta-c). Variations in palaeocurrent indicators is interpreted as a result of sediment transport in a confined setting, with deflections in the flow (sensu Kneller and McCaffrey, 1999). Bed amalgamations, inverse grading of the lower portion and missing fractions imply a proportion of these flows were bypassing and mud-clasts imply these flows had the ability to erode the sea-floor. |
| | Lithofacies 2: Lenticular thick-bedded sandstone<br>Description: Pale grey to beige irregularly bedded fine-grained sandstones up to 3 m thick. Bed bases are irregular, with decimetre scale incisions truncating underlying strata. Sole marks, primarily flute casts may scour into the underlying sediment. Beds variably show planar cross-stratification, extensive dewatering and convolute bedding, grading to planar lamination and ripple lamination at the bed tops or may be massive and contain abundant sand- and mud-clasts. Laminations are often highlighted by organic rich bands and carbonaceous debris up to 10 cm long. Amalgamation is common and beds typically show a lenticular form, thinning over tens of meters in width. Rarely beds are granular to medium grained and may have a significant glauconite and bioclastic component. Bioturbation is rare and occurs as large vertical burrows (e.g. *Ophiomorpha* sp.) at bed tops and fossils were only observed as broken shell fragments <1 cm. | Interpretation: These relatively coarser grained, often cross-stratified, lenticular beds are interpreted as the fill of low aspect ratio scours and / or small distributary channels by deposits of high-density turbidity currents (Normark et al., 1979). The structures and fill imply channel fills are the more likely (e.g. Kane et al., 2009; Prelat et al., 2009). The bioclastic and glauconitic bed bases implies that at least part of these flows initiated in a shallow marine environment, however the fact that the upper portions of these beds commonly show carbonaceous material and carbonized wood fragments implies some terrigenous mixing. |

| | | |
|---|---|---|
| | Lithofacies 3. Discontinuous thin- to medium-bedded sandstones and siltstones<br>Description: Pale grey to beige, well sorted, fine to very fine-grained sandstones overlain by siltstones, typically < 10 cm thick. Typically shows a sharp, irregular base, occasionally lower portion of beds show planar laminations and upper portions may show ripples and cross-lamination with siltstone. Beds are not necessarily normally graded and may show variation in the order of structures. Beds may show significant lateral variation in thickness, occurring as lenses, pinching-and swelling or thinning laterally. May be rich in carbonaceous material. Sandstones are typically texturally immature, displaying a variety of lithic fragments and glauconite. Bioturbation is variable but macrofossils were not observed. | Interpretation: Deposition from dilute, low-density turbidity currents (Bouma Tc-d-e). The presence of traction structures implies deposition from waning flows. The lateral variation may be a result of thinning and pinch out against a confining surface when apparent or to have infilled a scour surface. When filling scours these deposits may be inferred to have a bypass component, especially when grain size fractions are missing (*sensu* Stevenson et al., 2015). |
| | Lithofacies 4: Tabular thin- to medium-bedded sandstones, siltstones and mudstones<br>Description: Pale grey to beige, normally graded, typically well-sorted, fine to very fine grained sandstones typically <20 cm thick. Bed bases may be sharp or slightly irregular with sole marks including tool marks and flutes. The lower portion of beds may show planar lamination, often highlighted by carbonaceous rich bands; beds typically subtly grade up and often show a dewatered and or massive middle interval; bed tops are typically current rippled and grade to siltstone and mudstone; this is an idealised succession and beds may show a different order or not all of the structures. Ripples often show a subtly different orientation to sole structures and infrequently show variations between rippled horizons in the same bed (Fig. 8). These beds are tabular and may be traced over hundreds of meters across any one outcrop. Bioturbation is variably absent to intense, particularly in bed tops which may show a mottled texture. | Interpretation: These sandstones that grade to silt- and mudstones, with a variety of traction structures are interpreted as the deposition of fine grained sediments from low-density turbidity currents (Bouma Tb-c-d-e). The normal succession of structures and continuity of beds implies deposition from waning flows. Variations in palaeocurrent indicators is interpreted as a result of sediment transport in a confined setting, with deflections in the flow (*sensu* Kneller and McCaffrey, 1999). |

| | | |
|---|---|---|
| | Lithofacies 5: Alternation of sandstones and debrites<br>Description: In idealized sections immediately overlying thin-bedded (<10 cm), very fine-grained, often rippled horizons of "clean" sandstone, are medium bedded (20-60 cm) argillaceous sandstones, rich in floating mudstone clasts (up to 60%). Clasts are typically <20 cm long and less than 5 cm thick, sub-spherical and sub-elongate, but become more angular and elongate with increased size. These deposits are matrix supported, which normally consists of a "dirty" sandstone, rich in micaceous material, organic matter and occasionally bioclastic debris. These are typically overlain by a thin, argillaceous sandstone, although the overlying sandstone may be truncated by a subsequent deposit. | Interpretation: These sandwich beds are interpreted as hybrid event beds, *sensu* Haughton et al. (2003). The Initial clean sandstone may represent the head of the flow, which outran the erosive body, whilst delaminating the sea floor and entraining mud-clasts. This resulted in the body of the flow being deposited as a mud-clast rich debrite, over which the tail of the flow deposited a second, argillaceous sandstone. This is an idealised succession and all or parts of the event bed may be present depending upon run out distance, preservation etc. |
| | Lithofacies 6. Bioclastic grits<br>Description: Pale yellow to beige, often weathering orange thin-beds of granular to fine material, primarily comprising a poorly sorted mixture of siliciclastic, bioclastic and glauconite grains of variable proportions. Mud-clasts are also common, typically less than 5 cm long, but up to 50 cm. Exotic pebbles are a rare inclusion. Bed bases are typically sharp, erosive and may display sole marks. Beds are variably massive, show coarse laminations or planar cross-stratification. Beds are often very laterally variable in thickness, grain size and persistence, often seen to be pinching and swelling down dip. Bioclasts include mollusc fragments, foraminifera, bone material (primarily fish, but also cetacean), corals and other marine organisms. Although rare, terrestrial material, including wood fragments may also be found in these beds. These beds may occur in isolation within mudstone intervals, or more commonly immediately below much finer grained LF1, 3 and 4, or very rarely as lamina in normally graded beds. | Interpretation: These coarse, bioclastic beds are interpreted as the deposits of gravity flows originating from local shallow marine environments, reworking material from shelves to deposit them in relatively deep-water. Their common association with very fine grained material may be interpreted in one of two ways. 1) These beds were triggered simultaneously with finer siliciclastic rich events. Or 2) They represent a missing grain size (bypassed) portion in normally graded events. The observation of beds grading normally through medium and fine with decreasing bioclastic content implies the latter was the dominant process. These beds have been proposed as possible marker horizons across the basin by (Francis and Johansen, 2011) |

| | | |
|---|---|---|
| | Lithofacies 7. Massive, marine mudstone<br>Light to dark grey mudstone occurring in beds up to 75 cm thick, which can amalgamate into packages meters to tens of meters thick. Beds are typically laterally continuous over outcrop scale. Bedding may be recognised by broad colour changes and concreated horizons. Rarely isolated silt- or sandstone lamina may occur. Typically exhibits a blocky texture, with a conchoidal fracture. Rarely shows small biocoenotic macrofossils, such as *Inerocamerus* sp. molluscs or macro foraminifera (e.g. *Bathysiphon* sp.). Rare fragments of organic matter are often disseminated and it may show bioturbation, with horizontal burrows such as *Nerities* sp. and *Phycosiphon* sp. Large scale deformation in the form of slumps and slide scars is often evident. | Interpretation: This massive, blocky, mudstone is interpreted to represent background hemipelagic sedimentation in the marine environment. This may occur in shelf to deep-water settings. Isolated silt- or sandstone lamina may represent the very distal fine tail of a turbidity current passing elsewhere in the basin. Deformation implies deposition on an often unstable slope, with remobilisation of gravitationally unstable sediment. |

1324

1325

Table 2. Seismofacies of the trench-slope basin fill.

| Seismofacies | Amplitude & dimensions | Name and interpretation |
|---|---|---|
| 1 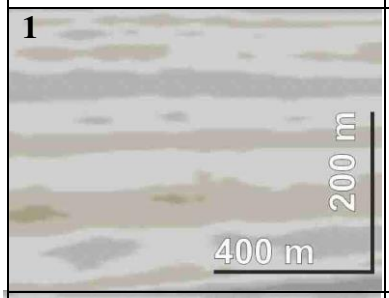  | Low amplitude, low frequency, laterally continuous (where not truncated or deformed). Tens to hundreds of meters thick, but thousands to tens of thousands wide. Here observed within the thrust-cored anticlines and overlying seismofacies 4. | Background deposits. These are interpreted to represent background, mudstone dominated sediments deposited at a time when coarser grained sediments were not being delivered to the study area (sensu Vinnels et al., 2010). |
| 2 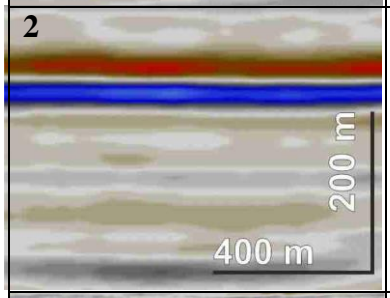  | Alternating high and low amplitude, low frequency packages seen to be thickening towards the core of troughs and onlapping at margins. Seen within the trench-slope basins underlying seismofacies 4. | Ponded deposits. These are interpreted as alternating sandstone and mudstones ponding within heavily confined areas of the slope (Prather et al., 1998) |
| 3 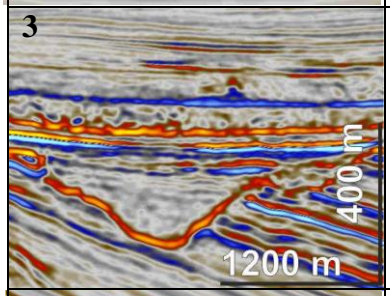  | Variable amplitude and frequency fill of lenticular incisions tens to hundreds of meters deep, by hundreds to thousands of meters wide, although typically less than 500 m wide. | Submarine channel fill. These incising features with variable fill are interpreted as submarine channel complexes (Mayall et al., 2010). These are seen to be conduits feeding both seismofacies 4 and 5 into the trench-slope basins. |
| 4 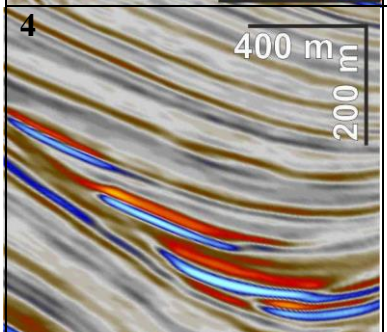  | Mixed amplitude, low frequency radial, mounded features kilometres wide by tens of meters thick, stacking into packages hundreds of meters thick. Internally, reflectors may downlap towards the lateral margins and horizon slices display intricate high amplitude fingers radiating from the upstream portion of this unit. | Lobe complexes. These mounded, radial reflectors are interpreted as deep-marine lobe complexes (Booth et al., 2003). The high amplitude lenses are interpreted as distributary channels within the lobe complex, some of which are seen to extend beyond the high amplitude portions, implying bypass. |
| 5 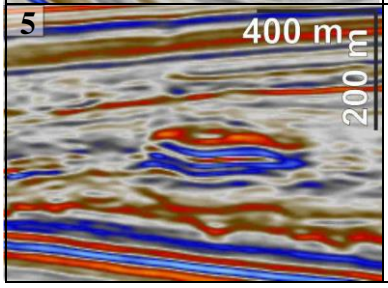  | Internally chaotic, irregular packages tens to hundreds of meters thick, often thousands of meters wide. Rarely coherent rafts or deformed packages of banded, high and low amplitude material can be seen internally. | MTDs. These chaotic geobodies are interpreted to represent MTDs (Posamentier and Kolla, 2003). These may be derived from the shelf or upper slope or local structures and may erode or block the system (Ortiz-Karpf et al., 2015). |

1326

1327

Table 3. Examples of anomalously thick, aggradational lobe complex dimensions, bounding conditions and origin.

| System | Amalgamated lobe complex thickness | Age (temporal span) | Type of margin | Inferred control | Authority |
|---|---|---|---|---|---|
| Gres d'Annot, Chalufy, SE France (outcrop) | 90 m | <30 Ma (Eocene – Oligocene) | Convergent, mini-basins | Sediment bypass in overfilled mini-basin | Joseph et al., 2000 |
| Cervarola Sandstone, Italian Appenines (outcrop) | 80 m, but generally not amalgamated | Miocene | Convergent, foredeep | Lateral structure growth | Tinterri and Piazza, 2019 |
| Mahia Peninsula, New Zealand (outcrop) | 385 m but intercalated with channel fill, MTDs and hemipelagites. | Late Miocene | Convergent, trench-slope basin | Migration of lobe complexes along axis of trench slope basin | Burgreen and Graham, 2014 |
| Marnoso-Arenacea, Italian Appenines (outcrop) | 20-40 m, but generally not amalgamated | Miocene | Convergent, foredeep | Increasing tectonic confinement | Tinterri and Tagliaferri, 2015 |
| Southern Hikurangi Margin, New Zealand (outcrop and subsurface) | 200 – 300 m | < 2 Ma | Convergent, trench-slope basin | Flow stripping over growing thrust structure | This study |
| Troika Field, Gulf of Mexico (subsurface) | 80 - 200 m | Unknown | Passive, salt tectonics mini-basin | Flow stripping at salt evacuation structure | Horine et al., 2000 |
| Active channel-mouth lobe complex, Congo-Angola margin (seafloor) | 20-70 m | Present day | Passive margin | Sediment flux | Dennielou et al., 2017 |

1328